Optimization of time domain induced polarization data acquisition and spectral information content

Per-Ivar Olsson

LUND
UNIVERSITY

Abstract

The need for detailed subsurface information is increasing due to city expansion and infill projects as well as subsurface construction projects. One common method for acquiring this geo-information is the direct current resistivity and time domain induced polarization method (DCIP) that measures the electrical resistivity and chargeability of the subsurface. The work presented in this thesis demonstrates that the usefulness of the DCIP method can be improved. Field time and cost efficiency is increased by means of waveform optimization and investigations of the effect of different current pulse on-time duration. Furthermore, post processing efficiency is increased as a result of improved data quality and reliability. Additionally, the available spectral information from DCIP surveys is substantially increased by enabling extraction of the IP response closer to the pulse than was previously possible. In combination with more accurate removal of background drift potential, which improves data quality at late times, the spectral information is further increased. In total, these optimizations increase the usefulness of the resistivity and (spectral) time domain induced polarization method and can hopefully contribute to spreading and intensifying its use for acquiring qualified subsurface information.

List of appended papers

The following three papers are appended in the thesis. The thesis author has conducted field data acquisition for the papers and developed major parts of the processing steps for the raw data. As the main author he has also been leading the writing of the papers. The modifications of the inversion software Aarhusinv related to on-time induced polarization was done by Gianluca Fiandaca.

Paper A

Olsson, P.-I., Dahlin, T., Fiandaca, G., Auken, E., 2015. Measuring time-domain spectral induced polarization in the on-time: decreasing acquisition time and increasing signal-to-noise ratio. Journal of Applied Geophysics. doi:10.1016/j.jappgeo.2015.08.009

Paper B

Olsson, P.-I., Fiandaca, G., Dahlin, T., Auken, E., 2015. Impact of Time-domain IP Pulse Length on Measured Data and Inverted Models, in: Near Surface Geoscience 2015 - 21st European Meeting of Environmental and Engineering Geophysics. doi:10.3997/2214-4609.201413755

Paper C

Olsson, P.-I., Fiandaca, G., Larsen, J.J., Dahlin, T., Auken, E., 2016. Doubling the spectrum of time-domain induced polarization: removal of non-linear self-potential drift, harmonic noise and spikes, tapered gating, and uncertainty estimation. to be submitted for publication (Geophysical Journal International).

Preface

The work of this thesis has been carried out at the Division of Engineering Geology, Lund University in Sweden and in part at the Hydrogeophysics group, Department of Geoscience at Aarhus University in Denmark.

I want to thank my main supervisor Torleif Dahlin and my assisting supervisors Gianluca Fiandaca and Esben Auken for excellent support, help and guidance. I would also like to thank Jakob Juul Larsen at the Signal processing group, Department of Engineering at Aarhus University.

Per-Ivar Olsson

January 2016

Contents

1 Introduction

The need for detailed information of the subsurface is increasing due to city expansion and infill projects as well as subsurface construction projects (e.g. tunnelling). One common method for acquiring this geo-information is the direct current resistivity and time domain induced polarization method (DCIP) which measures the electrical resistivity and chargeability of the subsurface (Dahlin, 2001; Loke et al., 2013). This thesis summarizes selected work on developing and increasing the usefulness of the DCIP method with focus on the induced polarization.

Electrical resistivity tomography (ERT) has been successfully used in a wide range of subsurface applications (Loke et al., 2013) such as environmental and engineering (Auken et al., 2014; Dahlin et al., 1999), hydrogeological (Auken et al., 2006; Fetter, 2001; Leroux and Dahlin, 2005) and archaeological (Argote-Espino et al., 2013; Florsch et al., 2011). However, different subsurface materials can have the same resistivity (Glover, 2015) and thus is it not possible to differentiate them when only using the resistivity information. This makes the chargeability information especially valuable since it can be measured simultaneously with the resistivity with little or no extra effort and the materials can have the same value for resistivity but different values for the chargeability. Hence, having two parameters reduces the ambiguity when relating the DCIP measurements to processes and geology. This reduction in ambiguity has been demonstrated for several applications, such as landfill mapping (Dahlin et al., 2010; Leroux et al., 2007) and lithology mapping (Kemna et al., 2004; Slater and Lesmes, 2002) and microbial activities (Slater et al., 2008),

The induced polarization phenomenon can be further evaluated by considering its frequency dependency, the spectral information. The frequency dependency is described with different models and, depending on the choice of model, additional parameters can be retrieved from the chargeability measurements so that the possible ambiguity can be reduced even more. The use of spectral IP information in engineering applications is still limited but there are several examples of research where the spectral information has proven useful. For example for aquifer characterization (Revil et al., 2015; Slater and Glaser, 2003), mapping geochemical changes (Doetsch et al., 2015a), permafrost monitoring

(Doetsch et al., 2015b) and landfill mapping (Gazoty et al., 2013, 2012a, 2012b).

Even if different levels of chargeability information generally can be retrieved from DCIP surveys, often only the resistivity parameters are evaluated in applied engineering investigations. This has several explanations, for example: older instruments with limited capability of successfully measuring the chargeability are still in use and knowledge of how the chargeability information should be interpreted could be missing. Another important factor is related to data quality, since the induced polarization measurement have much lower signal-to-noise ratio compared to the resistivity measurements, the data quality can be poor. Using the data would require more time for manual filtering of the data, and thus more money than can be allocated to make use of the chargeability data. This calls for an assessment on how to generally improve the quality of the acquired induced polarization data, and automated ways of data quality assessment and data filtering.

This spectral evaluation in turn demands a wide time-range of chargeability information (e.g. from one millisecond to several seconds) and even higher data quality than the regular "one parameter evaluation". Hence smart processing of the DCIP data is needed in order to allow a more widespread use of the method. Time and cost efficiency of spectral DCIP measurements is also limiting the usefulness of the method. The field measurements can require thousands of readings, where more data stacking and longer current transmission pulses may be required compared to what would be used in a regular DCIP survey. Thus there is a need for optimizing the measurement procedure to reduce the time and costs related to the field surveys.

1.1 Aim, objective and limitations

The aim of this study is to increase the usefulness of the DCIP method by developing the data acquisition and processing methodology. Therefore, the objectives of this study are to reduce acquisition time and costs, to increase data (spectral) information content, reliability and quality and to reduce the time and cost for data processing.

This work has not considered any other field surveying or geophysical method than the direct current resistivity and time domain induced polarization method. Additionally, the handling of electromagnetic coupling has not been considered as a part of this work except for applying an improved field procedure (Dahlin and Leroux, 2012). Furthermore, the work has focused on developing the time domain measurement technique rather than the frequency domain counterpart. Due to this is only a very brief overview given regarding the frequency domain measurements.

2 The DCIP method

DCIP measurements are carried out by injecting current into the subsurface between two electrodes while measuring the potential between one or several other pairs of electrodes (Figure 1) (Fink, 1990; Sumner, 2012; Zonge et al., 2005). The aim of the measurements is to get information of the electrical resistivity and chargeability of the subsurface. Information from different subvolumes of the subsurface is retrieved by repeating the measurements with different electrode combinations. With electrode combinations arranged along a line, one- or two-dimensional, depending on what combinations are used, information of the subsurface below the line can be retrieved. If the combinations instead cover an area it is possible to recover a three-dimensional information volume (Loke and Barker, 1996).
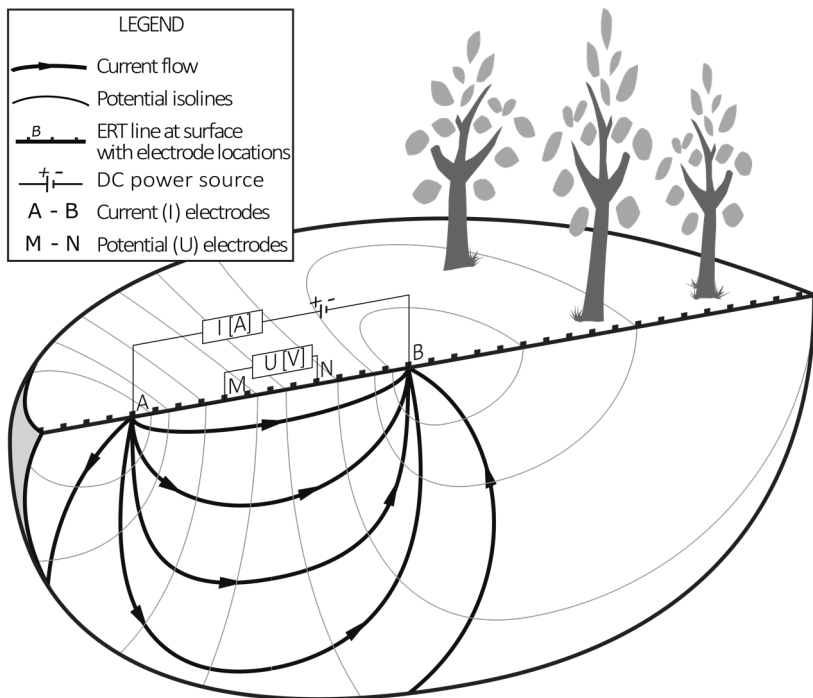

Figure 1. Schematic overview of 2D DCIP measurement principle on a homogenous subsurface. Original image provided by Nijland et al. (2010).

2.1 Resistivity

The resistivity (ρ, unit Ωm) is a material property that quantifies to what extent the material is opposing the flow of electrical current.

From the measurements (Figure 4) of the current (I) and potential (V_{DC}, Figure 2) is it possible to calculate the resistance (R) of the subsurface through Ohm's law:

$$R = \frac{V_{DC}}{I}$$

By also taking into account the geometry of the electrode placements (geometric factor, K) one may retrieve the apparent resistivity (ρ_a), which only corresponds to the true resistivity of the subsurface if it is homogenous and isotropic.

$$\rho_a = K \frac{V_{DC}}{I}$$

where

$$K = 2\pi (r_{AM}^{-1} - r_{BM}^{-1} - r_{AN}^{-1} + r_{BN}^{-1})^{-1}$$

and r denotes the different distances between current (A and B) and potential (M and N) electrodes. If the subsurface has a heterogeneous distribution of resistivities is it necessary to conduct a more advanced interpretation of the measurements to retrieve the resistivity of the subsurface, see 2.5 Inversion.

2.2 Chargeability

The chargeability (m_o, unit mV/V) is a material property that quantifies the capacity of the material to store energy.

The chargeability is defined as the ratio between the measured voltage following a sudden change in current ($V_{IP,o}$, Figure 2), normalized with the measured potential before the current change (V_{DC}) (Seigel, 1959):
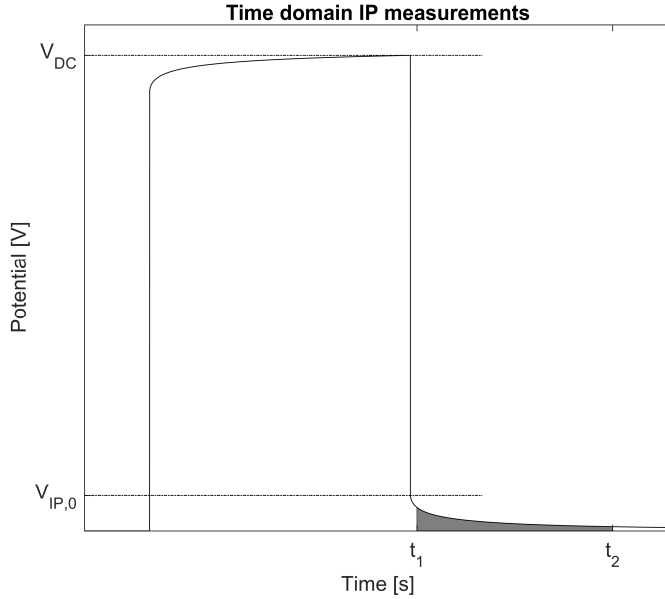
$$m_0 = \frac{V_{IP,0}}{V_{DC}}.$$

Figure 2. Theoretical full waveform potential for DCIP measurements with indication of parameters important for the data evaluation.

The chargeability is in time-domain determined by considering the transient potential response of the subsurface following a change in the injected current (Figure 2). It can be evaluated in several ways: for chargeability only (definition), for the mean chargeability within a given time interval (integral chargeability, m_{int}):

$$m_{int} = \frac{1}{V_{DC}\Delta t} \int_{t_1}^{t_2} V(t)dt$$

or for normalized integral chargeability (normalized with resistivity, see Slater and Lesmes (2002)) corresponding to surface polarization (Binley, 2015). Furthermore, the frequency characteristics of the potential response can be considered (spectral chargeability) by using different models for describing the shape (Figure 3) of the IP response (Johnson, 1984; Tombs, 1981), for example the Cole-Cole model in time-domain is described by (Florsch et al., 2011; Pelton et al., 1978; Revil et al., 2015):

$$V_{IP}(t) = m_0 \sum_{j=0}^{\infty} (-1)^j \left(\frac{t}{\tau}\right)^{jc} \Gamma(1+jc)^{-1}$$

for relaxation time (τ), frequency exponent (c) and Euler's Gamma function (Γ):

$$\Gamma(x) = \int_0^\infty y^{x-1} e^{-u} \, dy.$$

Analogous to resistivity and apparent resistivity it is not possible to directly retrieve the chargeability of the subsurface from the DCIP measurements unless it is homogenous in terms of chargeability, thus normally inversion is needed.
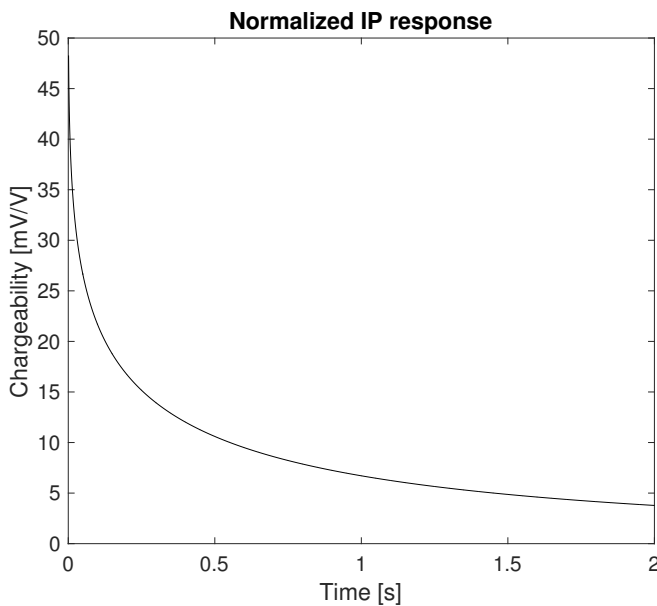
Figure 3. A normalized IP response generated from the modelled measurement seen in Figure 4.

2.3 Measurement waveforms

The current waveform injected into the ground differs depending on whether the measurements are conducted in time or frequency domain. Time domain measurements consider changes with time, while frequency domain measurements consider at what frequencies the changes take place. The two methods are theoretically equivalent but differ in terms of

measurement technique and actual capability to resolve the spectral IP parameters (Binley, 2015).

2.3.1 Time domain

Time domain measurements typically inject a 50% duty cycle square current waveform with constant current (Figure 4). The polarity of the current is reversed every pulse in order to remove background potentials superimposed on the signal measured between the receiver electrodes, caused by electrode polarization effects (Binley, 2015). Thus, at least two pulses with opposite sign are injected. This pulse train can be repeated (stacked) to retrieve multiple readings of the potential response and reduce the influence of noise (see 3 Measurement challenges).

The potential readings (V_{DC}, Figure 2) for calculating resistivity are taken as an average potential at the end of each current injection so that the potential has had time to stabilize and that prominent IP responses likely have worn off. For IP the potential readings are taken during the current off-time and the potential is normally averaged within predefined windows, starting at a fixed delay time after the current pulses. The time windows have increasing lengths and are normally chosen as multiples of the time period of the household power grid frequency (i.e. 50 Hz and 20 milliseconds in Sweden) to average out harmonic noise. The integral chargeability is determined as a weighted sum of the IP windows while for spectral IP all windows and timing information is required for the inversion.
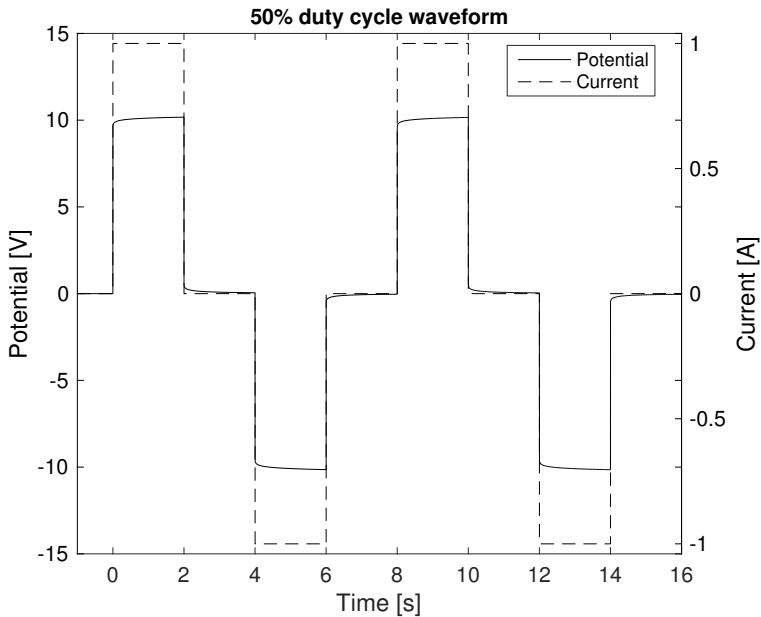
Figure 4. Injected current and modelled measured potential for the 50% duty-cycle waveform used for time domain DCIP measurements. Two stacks is achieved with 4 pulses and a current on-time of 2s. The corresponding stacked, averaged and normalized IP response can be seen in Figure 3.

2.3.2   Frequency domain

In frequency domain, current with a sine waveform of different frequencies is transmitted while the resistivity and IP information is retrieved as the amplitude and phase shift of the measured potential respectively (Binley, 2015; Florsch et al., 2011). By having a narrow passband filter corresponding to the frequency of the current transmitted it is possible to filter out background drift (~DC), harmonic noise (by avoiding transmitting at harmonic noise frequencies or its harmonics) and in part also the spikes.

2.4 Time or frequency domain?

Many technical measurement issues related to different noise sources (see 3 Measurement challenges) can be avoided if the measurements are carried out in frequency domain instead of in time domain. Furthermore, it should be noted that extracting spectral IP parameters (e.g. Cole-Cole)

from time-domain measurements theoretically assumes that all polarization processes have been saturated and that early decay times (<400 milliseconds) might be affected by non-desirable processes such as Maxwell-Wagner polarization and electromagnetic coupling (Revil et al., 2015). However, the frequency domain measurements are highly time consuming compared to the time domain counterpart and consequently rarely used in commercial engineering and environmental applications but mainly used for research purposes. Since this work is aiming at techniques that can be expected to be adapted for routine practical applications it focuses on developing time domain measurements and on pushing the limit of the available spectral IP information from direct current resistivity and time domain induced polarization measurements.

2.5 Inversion

Inversion is an iterative process that aims to find a parameter model that gives synthetic measurements (forward response) that are similar to the real measurements. During the process the measured data are compared with the forward response for a known distribution of parameters (e.g. resistivity and chargeability) and the parameter values are changed until the responses are similar to the real measurements (Binley, 2015; Günther et al., 2006; Loke and Barker, 1996; Rücker et al., 2006).

Depending on the type of inversion, different numbers of parameters are used for describing the model space. For example, with the spectral chargeability Cole-Cole model four parameters are used: resistivity, chargeability, relaxation time and frequency exponent, where the latter three describes the shape of the IP response (Fiandaca et al., 2013, 2012; Hönig and Tezkan, 2007).

The time domain spectral chargeability inversion software described by Fiandaca et al. (2012 and 2013) models the waveform of current and potential, computes the forward response in frequency domain and transforms the response into time domain for comparing the measured data with the modelled response.

3 Measurement challenges

In field DCIP measurements the measured potentials are a mix of different sources (Figure 5), including the desired ground response of the current injection:

$$u_{measured} = u_{response} + u_{drift} + u_{harmonic\ noise} + u_{spikes} + u_{other}$$

To get an accurate determination of the potential response ($u_{response}$) it is essential to determine and compensate for as many of these sources as possible.

Figure 5. Different kinds of known sources that affect the measured potential and their typical signal characteristics: electrical fence - spikes (top left), power grid – harmonic noise (top right), tram running on DC – background drift (bottom left), DCIP instrument – square pulse train (bottom right).

3.1 Background drift

Background drift in DCIP data can have multiple origins, for example natural potential difference in the subsurface, natural electrode polarization (can be reduced using so called non-polarizable electrodes) and current induced electrode polarization (if using same electrodes for injecting current and measuring potentials). The drift is seen as a slow changing potential variation in the full waveform potential recording (Figure 6). If not corrected for, the drift can corrupt both resistivity and chargeability data but it is especially the tail of the IP response that is sensitive, due to its low signal-to-noise ratio, and thus mainly the spectral IP is affected. The correction for the drift is commonly done with a linear approximation (Dahlin et al., 2002; Peter-Borie et al., 2011).
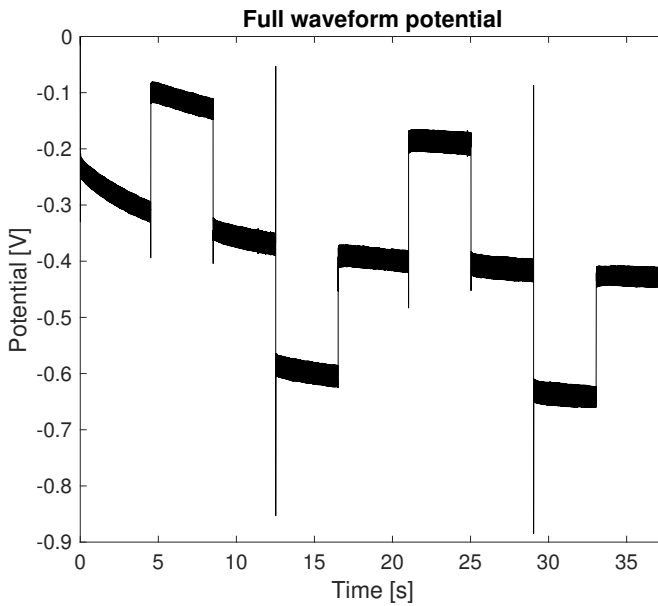
Figure 6. Example of full waveform potential recording that exhibits a clear background drift.

3.2 Spikes

Spikes (Figure 7) originating from anthropogenic sources, such as electrical fences for livestock management, can be registered by DCIP measurements. These spikes can cause problems when extracting DC (resistivity) and especially, due to its low signal-to-noise ratio, IP information from measured field data.

Figure 7. Example of full waveform potential recording with multiple spikes present.

3.3 Harmonic noise

Harmonic noise originates from the power supply sources oscillating at a base frequency (e.g. 50 Hz or 60 Hz) and harmonics of this base frequency (Figure 8 and Figure 9). In DCIP processing today, this is handled by averaging and gating over a full period of the known base frequency (e.g. 1/50 s or 1/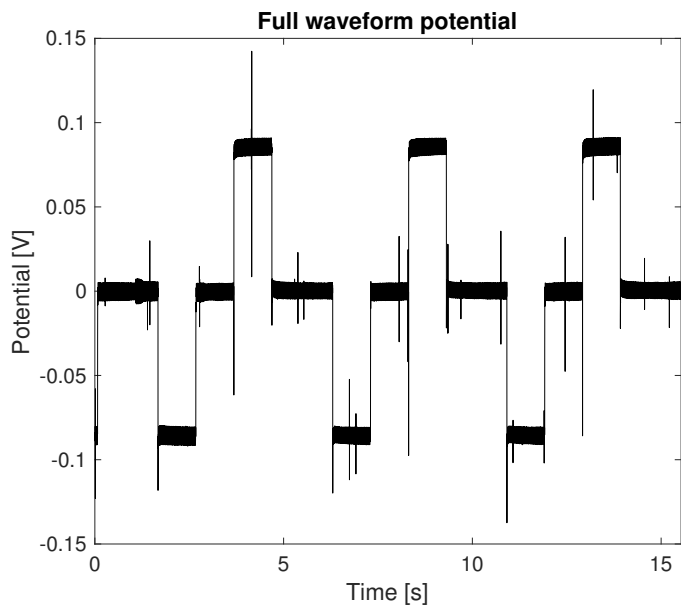60 s) for suppressing household power supply frequencies at 50 Hz and its harmonics. However, the need for long gates causes a loss of early IP response information close to current pulse change and thus makes it more difficult to resolve spectral parameters. This is especially severe when conducting field measurements close to electric railways in some countries (e.g. Austria, Germany, Norway, Sweden, Switzerland and USA) where the frequency of the power supply for the trains are even lower (16 2/3 Hz or 25 Hz).
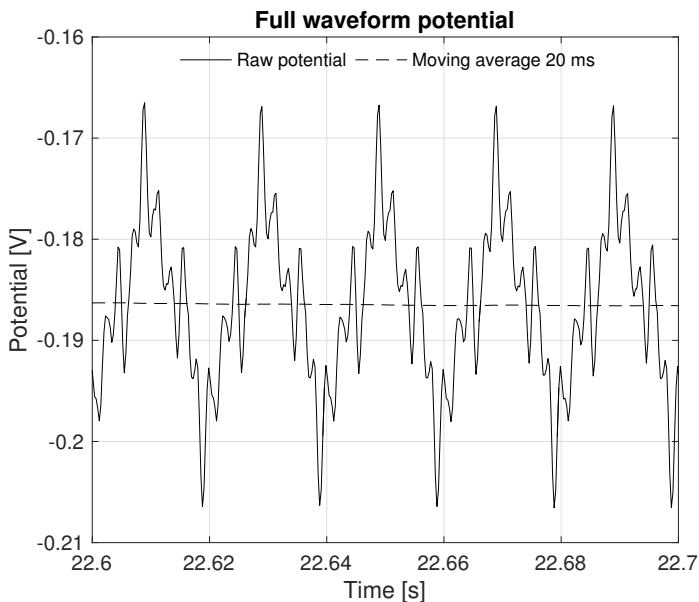

Figure 8. A magnification of the full waveform potential recording in Figure 6 and a moving average (20 millisecond window) version of the same signal. With the magnification the harmonic oscillations are clearly visible. The main oscillation has a time period of around 20 milliseconds.
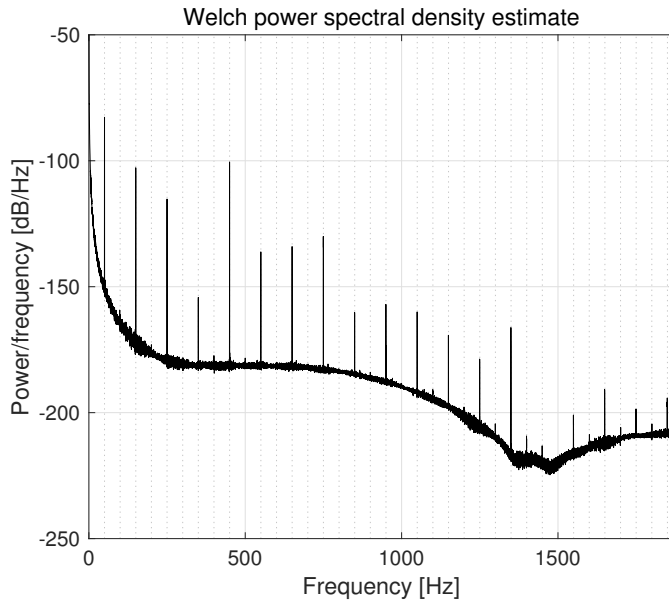
Figure 9. Welch power spectral density estimate for the time domain raw potential signal shown in Figure 6. The periodic reoccurring energy peaks suggest that harmonic noise from the power grid is present in the signal.

3.4 Electromagnetic coupling

Field surveys conducted with multicore cables where the potential and current wires are bulked in the same cable, as shown in Figure 1, generally suffer from different forms of electromagnetic (EM) coupling (Dahlin and Leroux, 2012). Handling of EM coupling is not a focus of this work, hence only a very brief overview is given here, but it should be noted that the coupling generally increases for longer arrays, lower resistivities and higher frequencies (Butler, 2005).

3.4.1 Capacitive coupling

Capacitive coupling can be defined as current leaks from high-potential surfaces or conductors to low-potential surfaces or conductors (Dahlin and Leroux, 2012). With a single multicore cable three main capacitive couplings can occur (Dahlin and Leroux, 2012; Radic, 2004): coupling between current and potential wire, coupling between the different

current wires (*A* and *B*) and coupling between current wire and the subsurface.

The main coupling effect is the one occurring between current and potential wires (Radic, 2004). One method to reduce this coupling is to increase the distance between the current and potential wires by using two multicore cables (Figure 10), one for current transmission and the other for potential measurements (Dahlin and Leroux, 2012).
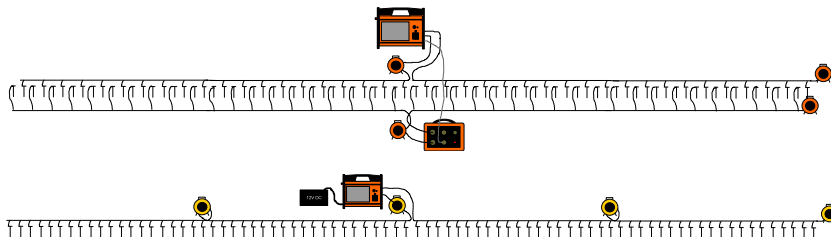
Figure 10. Example of measurement setup with two multicore cables (top). One cable and every second electrode is used for current injections while the remaining cable and electrodes are used for measuring potentials. By increasing the distance between current and potential wire the capacitive coupling between the two is reduced. Example of the traditional setup is provided for comparison (bottom). Image adapted from original by Torleif Dahlin.

3.4.2 Inductive coupling

Inductive coupling operates through magnetic fields and thus differs in origin from the capacitive coupling. It is possible to compensate for this coupling by means of modeling and also include it in the inversion (Ingeman-Nielsen and Baumgartner, 2006) but since focus of this work has been elsewhere this has not been considered in this work.

4 Main results

4.1 Paper A

Paper A concerns current waveform optimization to reduce acquisition time and increase signal-to-noise ratio.

Combined resistivity and time-domain direct current induced polarization (DCIP) measurements are traditionally carried out with a 50% duty cycle current waveform, taking the resistivity measurements during the on-time and the IP measurements during the off-time. One drawback with this method is that only half of the acquisition time is available for resistivity and IP measurements, respectively. In this paper, this limitation is solved by using a current injection with 100% duty cycle (Figure 11) and also taking the IP measurements in the on-time. With numerical modeling of current waveforms with 50% and 100% duty cycles the paper shows that the waveforms have comparable sensitivity for the spectral Cole–Cole parameters and that signal level is increased up to a factor of two if the 100% duty cycle waveform is used. The inversion of field data acquired with both waveforms (Figure 12) confirms the modeling results and shows that it is possible to retrieve similar inversion models with either of the waveforms when inverting for the spectral Cole–Cole parameters with the waveform of the injected current included in the forward computations.
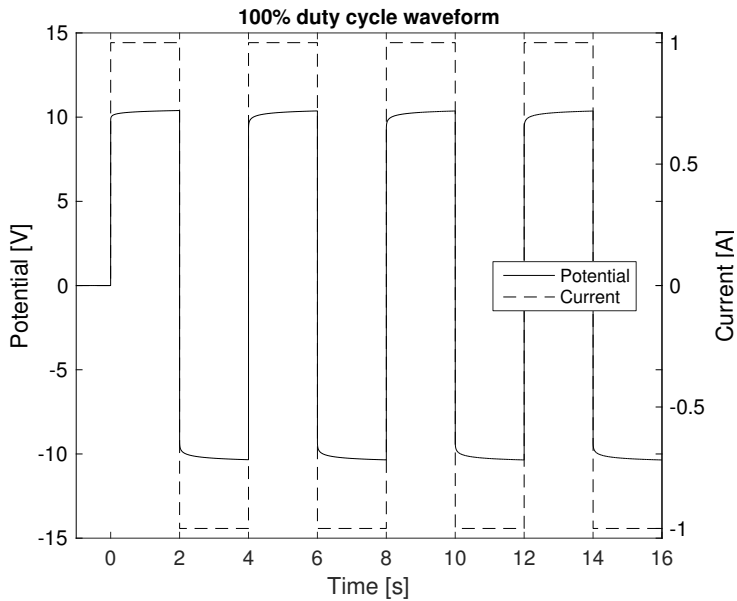
Figure 11. Showing injected current and modelled measured potential for the 100% duty-cycle waveform for time domain DCIP measurements.

The results show that on-time measurements of IP can reduce the acquisition time by up to 50% and increase the signal-to-noise ratio by up to 100% almost without information loss. The findings can contribute and have a large impact for DCIP surveys in general, and especially for surveys where time (and cost) efficiency and reliable data quality are important factors. Specifically, the findings are of value for DCIP surveys conducted in urban areas where anthropogenic noise is an issue and the heterogeneous subsurface demands time-consuming 3D acquisitions.
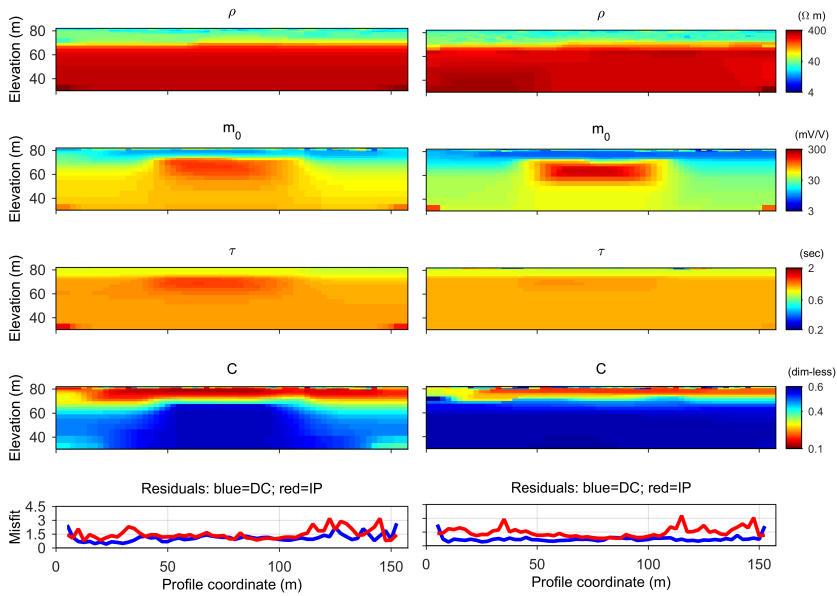
Figure 12. Inverted section and data misfit for field fata acquired with the 50% (left) and 100% (right) duty cycle current waveform.

4.2 Paper B

Paper B concerns the current injection duration and how this relates to resulting data, signal-to-noise ratio and inversion models.

The duration of time domain (TD) induced polarization (IP) current injections has significant impact on the acquired IP data as well as on the inversion models, if the standard evaluation procedure is followed. However, it is still possible to retrieve similar inversion models if the waveform of the injected current and the IP response waveform are included in the inversion. The on-time also generally affects the signal-to-noise ratio (SNR) where an increased on-time gives higher SNR for the IP data.

The commonly applied inversion of the induced polarization data only considers the integral chargeability, without taking the waveform of the injected current or the waveform of the IP response into account. The results show that, with these full waveform considerations included in the inversion, it is possible to retrieve similar inversion models for the

induced polarization, independent of the on-time duration. Furthermore, the results show that the signal-to-noise ratio (SNR) for the IP information increases with increasing duration of the current injections.
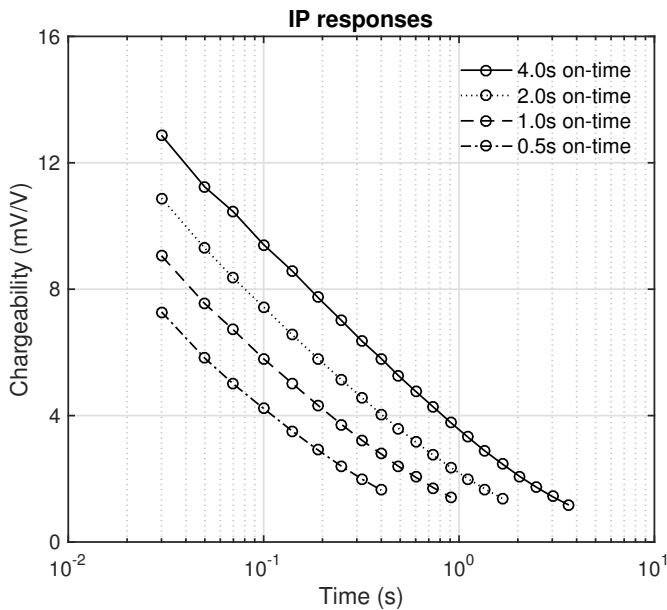
Figure 13. Acquired field IP decays corresponding to the same quadruple from each of the four data sets with different on- time. Note that the magnitude of the decays is increasing with longer on-time.

The results show that the on-time of the injected current has a substantial effect on retrieved induced polarization field data (Figure 13). It is clear from the results that this difference in data also affects the inverted subsurface IP models when using an inversion software that only considers integral chargeability Figure 14. However the results also show that it is in fact possible to retrieve similar inversion models given that the waveform of the injected current and the IP response waveform are included in the inversion (Figure 14) and that increasing on-time gives higher SNR for the IP data (Figure 13).
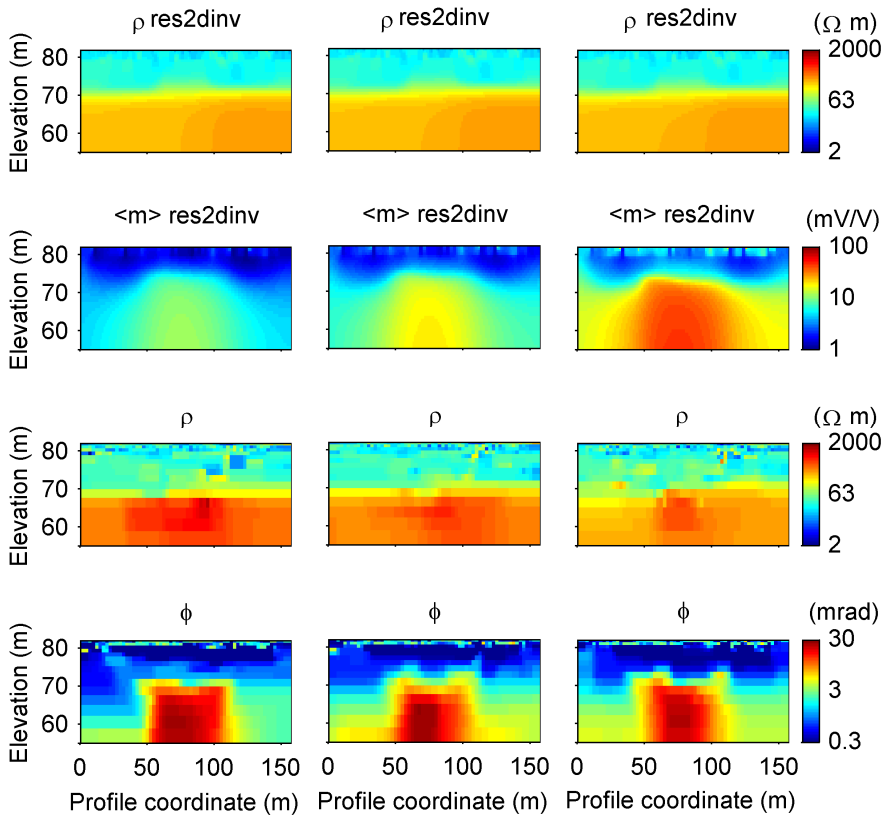
Figure 14. Inversion results from Res2dinv (two top rows) and Aarhusinv (two bottom rows) for different on-time (from left to right: 1, 2 and 4 seconds). The chargeability model from Res2dinv is clearly dependant on current on-time while the Aarhusinv (which include the current and potential waveforms in the inversion) models are more similar for the different on-times.

Only considering the integral chargeability can be misleading and likely makes it more ambiguous when trying to relate the IP models to processes and geology or preciously reported integral chargeability values. Furthermore, if not including the full waveform in the inversion, care needs to be taken that the same acquisition settings are used when making complimentary, verification or time-lapse measurements so that different data sets will be comparable in data and model space.

4.3 Paper C

This paper concerns signal processing of full waveform DCIP data and handles measurement issues such as IP gate distribution, spikes, harmonic noise and background drift. The improved handling of these issues doubles the spectral information content of DCIP data by enabling shorter gates than the traditional method (multiple of the time period of the harmonic noise) and by accurately recovering the shape of the IP response at late times.

The normally used linear drift correction is for DC and integral chargeability measurements often good enough but when evaluating the spectral IP information a more accurate approximation is needed. This paper applies a Cole-Cole model based background drift estimate (Figure 15 and Figure 18, top) which substantially improves the handling of non-linear drift cases such as current induced electrode polarization and especially improves late times of the IP response with low signal-to-noise ratio.
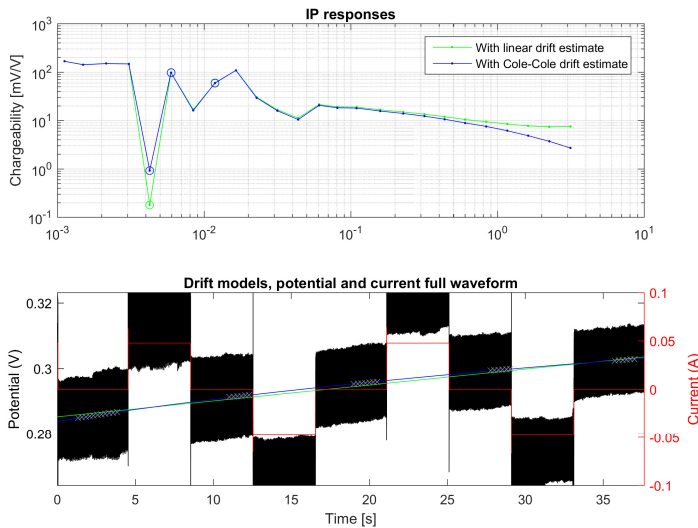
Figure 15. Showing 50% duty cycle raw full waveform potential (black) and current (red), subset of the signal used for finding the drift model (grey cross marker) and different types of background drift models (bottom). The resulting gated IP-response curves (green-linear model, blue-Cole-Cole model. Negative values are marked with circles) are shown in the top plot. Note that especially the end of the IP response is sensitive to the choice of drift model due to its low signal-to-noise ratio.

De-spiking is implemented by applying a series of filters on the full waveform potential for enhancing the spikes and generating a flexible and data-driven threshold value for spike rejection (Figure 16). The values of the identified spike samples are replaced based on the values of neighbouring non-spike samples.
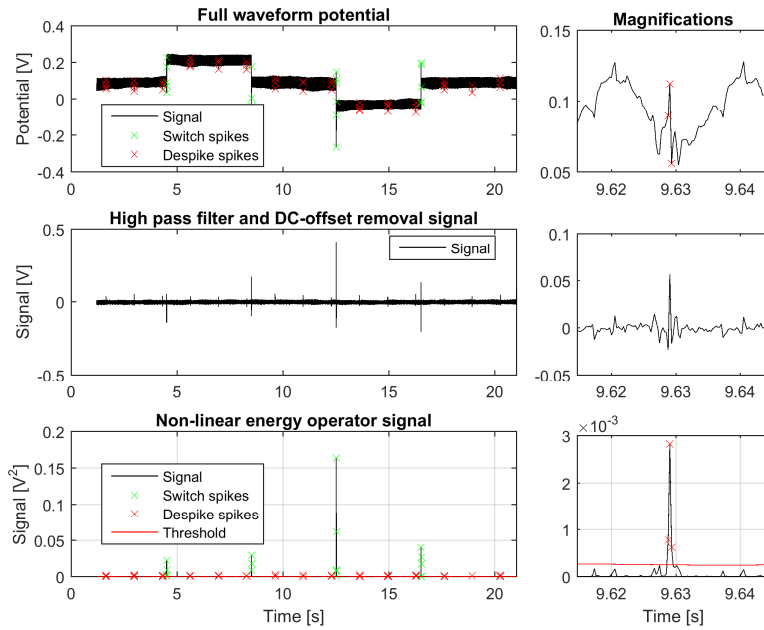
Figure 16. Showing identified spike samples of a full waveform potential signal (top), output from applied high pass and DC-offset removal filter (mid) and output from non-linear energy operator filter, spike samples and threshold value (bottom). Magnifications of the 7th identified despike spike (from 9.615 to 9.645 s) are shown on the right.

Cancelling of harmonic noise is implemented as a model based approach where the noise is described as a sum of harmonic signals. The different harmonic signals have frequencies given by a common fundamental frequency (f_0) multiplied with an integer (m) to describe the different harmonics but have independent amplitude (A_m) and phase ($_m$) for each harmonic m:

$$u_{harmonic\ noise}(n) = \sum_m A_m \cos(2\pi m f_0 n + \varphi_m)$$

with sample number n.

Since the harmonic noise is not stationary for an entire data acquisition (varying in phase, amplitude and frequency), the raw full waveform potential is segmented. Noise model parameters are determined for each segment in an iterative approach by minimizing the residual energy after subtraction of a temporary harmonic noise model. After finding the best noise model, the raw full waveform potential is corrected accordingly, which substantially reduces the energy of the harmonic noise (Figure 17).

The model based cancelling of harmonic noise reduces the need for gating with multiples of 20 ms (for 50 Hz) to supress the harmonic noise. Hence an improved gate distribution design can be applied with arbitrary gate widths, both shorter than 20 ms and multiples of 20 ms when feasible. This design in turn gives access to spectral information of the IP response closer to time zero which were unavailable with the traditional gating (Figure 18). In total, the first useable gate is one decade in time closer to time zero with the improved gate distribution design and model based noise cancelling compared to when applying the traditional method for handling the harmonic noise.
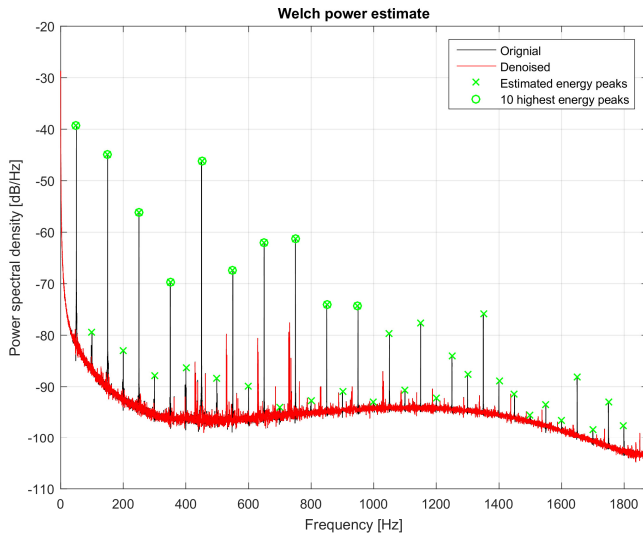
Figure 17. Welch power estimate of full waveform potential: original signal (black), residual signal after noise cancellation (red). The green markers show identified energy peaks (cross) and harmonics used for finding the noise model (circle). The remaining energy peaks are not harmonics of the 50 Hz.
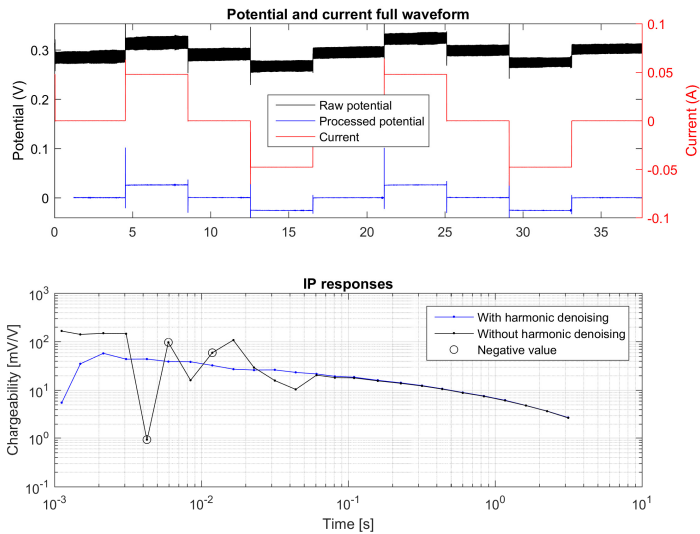
Figure 18. Showing full waveform current (red) and potential before (black) and after (blue) drift removal and cancelling of harmonic noise. The resulting IP response with harmonic de-noising (bottom, blue line) shows clear improvement of the erratic behaviour of the IP response.

5 Conclusions

The work presented in this thesis demonstrates that the usefulness of the DCIP method can be improved. Field time and cost efficiency are increased by means of current pulse on-time and waveform optimization. Additionally, post processing efficiency increases as a result of improved data quality and reliability. Furthermore, the available spectral information from DCIP surveys is substantially increased by enabling extraction of the IP response closer to the pulse than was previously possible. In combination with more accurate removal of background drift potential that can handle non-linear drift cases, the data quality is improved at late times and the spectral information content is further increased.

This work has focused on time-domain resistivity and spectral IP measurements. However, it is still unclear if the time-domain measurements can resolve the spectral parameters equally well as the frequency domain counterpart. Furthermore, even if the work has substantially increased data quality for the spectral IP, it still demands extensive work of manual quality assurance and filtering of the IP response data to enable successful interpretations and inversions. Hence there is scope for further development related to data quality and data processing.

6 Future research

As indicated in the conclusion, there still remain many issues to be solved for truly enabling the use of spectral DCIP information as a standard tool in applied engineering applications.

6.1 Data quality

There are some field cases where noise sources that have a large effect on the measured potential cannot be handled by the processing routine described in Paper C. Specifically, one noise source like this could be electrical vehicles running on DC (e.g. trams) generating a slowly varying DC offset with similar time-scale as the IP responses. Another problematic noise source can be trains running on AC passing close to a field survey generating harmonic noise with a fast varying amplitude and phase, possibly too fast for being modeled with the current implementation of the harmonic de-noising described by Paper C.

One possible approach to this issue could be to use differential measurements by separately measuring and compensating accordingly for these noise sources. This reference technique has been successfully applied in previous research but only for few electrode combinations (Halverson et al., 1989; Radic, 2014).

6.2 Post processing

Spectral IP evaluation still demands large amounts of manual processing and filtering of erroneous data points before inversion is possible. With increasing data sets, typically thousands of electrode combinations and 20-30 IP windows, there is a need for automatic processing and filtering of the IP response data. To enable this, it is crucial to first determine the possible theoretical shape IP responses from time domain spectral IP measurements, for example by means of numerical modelling.

7 References

Argote-Espino, D., Tejero-Andrade, A., Cifuentes-Nava, G., Iriarte, L., Farías, S., Chávez, R.E., López, F., 2013. 3D electrical prospection in the archaeological site of El Pahñú, Hidalgo State, Central Mexico. Journal of Archaeological Science 40, 1213–1223. doi:10.1016/j.jas.2012.08.034

Auken, E., Doetsch, J., Fiandaca, G., Christiansen, A.V., Gazoty, A., Cahill, A.G., Jakobsen, R., 2014. Imaging subsurface migration of dissolved CO_2 in a shallow aquifer using 3-D time-lapse electrical resistivity tomography. Journal of Applied Geophysics 101, 31–41. doi:10.1016/j.jappgeo.2013.11.011

Auken, E., Pellerin, L., Christensen, N.B., Sørensen, K., 2006. A survey of current trends in near-surface electrical and electromagnetic methods. Geophysics 71, 249–260. doi:10.1190/1.2335575

Binley, A., 2015. Tools and Techniques: Electrical Methods, in: Treatise on Geophysics. Elsevier, pp. 233–259. doi:10.1016/B978-0-444-53802-4.00192-5

Butler, D.K., 2005. Near-surface geophysics. Society of Exploration Geophysicists Tulsa.

Dahlin, T., 2001. The development of DC resistivity imaging techniques. Computers & Geosciences 27, 1019–1029.

Dahlin, T., Bjelm, L., Svensson, C., 1999. Use of electrical imaging in site investigations for a railway tunnel through the Hallandsås Horst, Sweden. Quarterly Journal of Engineering Geology & Hydrogeology 32, 163–173.

Dahlin, T., Leroux, V., 2012. Improvement in time-domain induced polarization data quality with multi-electrode systems by separating current and potential cables. Near Surface Geophysics 10, 545–656. doi:10.3997/1873-0604.2012028

Dahlin, T., Leroux, V., Nissen, J., 2002. Measuring techniques in induced polarisation imaging. Journal of Applied Geophysics 50, 279–298. doi:10.1016/S0926-9851(02)00148-9

Dahlin, T., Rosqvist, H., Leroux, V., 2010. Resistivity-IP mapping for landfill applications. First Break 28.

Doetsch, J., Fiandaca, G., Auken, E., Christiansen, A.V., Cahill, A.G., 2015a. Field-scale time-domain spectral induced polarization monitoring of geochemical changes induced by injected CO_2 in a shallow aquifer. Geophysics 16, 10294. doi:10.1190/geo2014-0315.1

Doetsch, J., Ingeman-Nielsen, T., Christiansen, A. V., Fiandaca, G., Auken, E., Elberling, B., 2015b. Direct current (DC) resistivity and induced polarization (IP) monitoring of active layer dynamics at high temporal resolution. Cold Regions Science and Technology 119, 16–28. doi:10.1016/j.coldregions.2015.07.002

Fetter, C.W., 2001. Applied hydrogeology. Prentice Hall, Upper Saddle River N.J.

Fiandaca, G., Auken, E., Christiansen, A.V., Gazoty, A., 2012. Time-domain-induced polarization: Full-decay forward modeling and 1D laterally constrained inversion of Cole-Cole parameters. Geophysics 77, E213–E225. doi:10.1190/geo2011-0217.1

Fiandaca, G., Ramm, J., Binley, A., Gazoty, A., Christiansen, A.V., Auken, E., 2013. Resolving spectral information from time domain induced polarization data through 2-D inversion. Geophysical Journal International 192, 631–646. doi:10.1093/gji/ggs060

Fink, J.B., 1990. Induced polarization: applications and case histories. Soc of Exploration Geophysicists.

Florsch, N., Llubes, M., Téreygeol, F., Ghorbani, A., Roblet, P., 2011. Quantification of slag heap volumes and masses through the use of induced polarization: application to the Castel-Minier site. Journal of Archaeological Science 38, 438–451. doi:10.1016/j.jas.2010.09.027

Gazoty, A., Fiandaca, G., Pedersen, J., Auken, E., Christiansen, A. V, 2012a. Mapping of landfills using time-domain spectral induced polarization data: The Eskelund case study. Near Surface Geophysics 10, 575–586. doi:10.3997/1873-0604.2012046

Gazoty, A., Fiandaca, G., Pedersen, J., Auken, E., Christiansen, A. V, 2013. Data repeatability and acquisition techniques for time-domain spectral induced polarization. Near Surface Geophysics 391–406. doi:10.3997/1873-0604.2013013

Gazoty, A., Fiandaca, G., Pedersen, J., Auken, E., Christiansen, A. V., Pedersen, J.K., 2012b. Application of time domain induced

polarization to the mapping of lithotypes in a landfill site. Hydrology and Earth System Sciences 16, 1793–1804. doi:10.5194/hess-16-1793-2012

Glover, P.W.J., 2015. Geophysical Properties of the Near Surface Earth: Electrical Properties, Treatise on Geophysics. Elsevier B.V. doi:10.1016/B978-0-444-53802-4.00189-5

Günther, T., Rücker, C., Spitzer, K., 2006. Three-dimensional modelling and inversion of dc resistivity data incorporating topography - II. Inversion. Geophysical Journal International 166, 506–517. doi:10.1111/j.1365-246X.2006.03011.x

Halverson, M.O., Kingman, J.E.E., Corbet, D., 1989. Advances in IP technology, telluric cancellation and high spatial resolution arrays, in: Exploration'87 Symposium, Toronto, Geol. Survey of Canada Publication. pp. 183–190.

Hönig, M., Tezkan, B., 2007. 1D and 2D Cole-Cole-inversion of time-domain induced-polarization data. Geophysical Prospecting 55, 117–133. doi:10.1111/j.1365-2478.2006.00570.x

Ingeman-Nielsen, T., Baumgartner, F., 2006. Numerical modelling of complex resistivity effects on a homogenous half-space at low frequencies. Geophysical Prospecting 54, 261–271. doi:10.1111/j.1365-2478.2006.00532.x

Johnson, I.M., 1984. Spectral induced polarization parameters as determined through time-domain measurements. Geophysics 49, 1993–2003. doi:10.1190/1.1441610

Kemna, A., Binley, A., Slater, L., 2004. Crosshole IP imaging for engineering and environmental applications. Geophysics 69, 97–107. doi:10.1190/1.1649379

Leroux, V., Dahlin, T., 2005. Time-lapse resistivity investigations for imaging saltwater transport in glaciofluvial deposits. Environmental Geology 49, 347–358. doi:10.1007/s00254-005-0070-7

Leroux, V., Dahlin, T., Svensson, M., 2007. Dense resistivity and induced polarization profiling for a landfill restoration project at Harlov, Southern Sweden. Waste Management & Research 25, 49–60. doi:10.1177/0734242X07073668

Loke, M.H., Barker, R.D., 1996. Practical techniques for 3D resistivity surveys and data inversion1. Geophysical Prospecting 44, 499–523. doi:10.1111/j.1365-2478.1996.tb00162.x

Loke, M.H., Chambers, J.E., Rucker, D.F., Kuras, O., Wilkinson, P.B., 2013. Recent developments in the direct-current geoelectrical imaging method. Journal of Applied Geophysics 95, 135–156. doi:10.1016/j.jappgeo.2013.02.017

Nijland, W., van der Meijde, M., Addink, E.A., de Jong, S.M., 2010. Detection of soil moisture and vegetation water abstraction in a Mediterranean natural area using electrical resistivity tomography. CATENA 81, 209–216. doi:10.1016/j.catena.2010.03.005

Pelton, W.H., Ward, S.H., Hallof, P.G., Sill, W.R., Nelson, P.H., 1978. Mineral discrimination and removal of inductive coupling with multifrequency IP. Geophysics 43, 588–609. doi:10.1190/1.1440839

Peter-Borie, M., Sirieix, C., Naudet, V., Riss, J., 2011. Electrical resistivity monitoring with buried electrodes and cables: noise estimation with repeatability tests. Near Surface Geophysics 9, 369–380. doi:10.3997/1873-0604.2011013

Radic, T., 2004. Elimination of Cable Effects while Multi-Channel SIP Measurements, in: Near Surface 2004 - 10th EAGE European Meeting of Environmental and Engineering Geophysics.

Radic, T., 2014. Geoelectric Reference Technique, Efficient Tool to Eliminate External Noise in SIP Data, in: Near Surface Geoscience 2014 - 20th European Meeting of Environmental and Engineering Geophysics. doi:10.3997/2214-4609.20141984

Revil, A., Binley, A., Mejus, L., Kessouri, P., 2015. Predicting permeability from the characteristic relaxation time and intrinsic formation factor of complex conductivity spectra. Water Resources Research 51, 6672–6700. doi:10.1002/2015WR017074

Rücker, C., Günther, T., Spitzer, K., 2006. Three-dimensional modelling and inversion of dc resistivity data incorporating topography - I. Modelling. Geophysical Journal International 166, 495–505. doi:10.1111/j.1365-246X.2006.03010.x

Seigel, H.O., 1959. Mathematical formulation and type curves for induced polarization. Geophysics 24, 547–565. doi:10.1190/1.1438625

Slater, L., Ntarlagiannis, D., Yee, N., O'Brien, M., Zhang, C., Williams, K.H., 2008. Electrodic voltages in the presence of dissolved sulfide: Implications for monitoring natural microbial activity. Geophysics. doi:10.1190/1.2828977

Slater, L.D., Glaser, D.R., 2003. Controls on induced polarization in sandy unconsolidated sediments and application to aquifer characterization. Geophysics. doi:10.1190/1.1620628

Slater, L.D., Lesmes, D., 2002. IP interpretation in environmental investigations. Geophysics 67, 77. doi:10.1190/1.1451353

Sumner, J.S., 2012. Principles of induced polarization for geophysical exploration. Elsevier.

Tombs, J.M.., 1981. The feasibility of making spectral IP measurements in the time domain. Geoexploration 19, 91–102. doi:10.1016/0016-7142(81)90022-3

Zonge, K.L., Wynn, J., Urquhart, S., 2005. 9. Resistivity, Induced Polarization, and Complex Resistivity, in: Near-Surface Geophysics. pp. 265–300. doi:10.1190/1.9781560801719.ch9

8 Appended papers

Paper A

Olsson, P.-I., Dahlin, T., Fiandaca, G., Auken, E., 2015. Measuring time-domain spectral induced polarization in the on-time: decreasing acquisition time and increasing signal-to-noise ratio. Journal of Applied Geophysics. doi:10.1016/j.jappgeo.2015.08.009

Paper B

Olsson, P.-I., Fiandaca, G., Dahlin, T., Auken, E., 2015. Impact of Time-domain IP Pulse Length on Measured Data and Inverted Models, in: Near Surface Geoscience 2015 - 21st European Meeting of Environmental and Engineering Geophysics. doi:10.3997/2214-4609.201413755

Paper C

Olsson, P.-I., Fiandaca, G., Larsen, J.J., Dahlin, T., Auken, E., 2016. Doubling the spectrum of time-domain induced polarization: removal of non-linear self-potential drift, harmonic noise and spikes, tapered gating, and uncertainty estimation. to be submitted for publication (Geophysical Journal International).

8.1 Paper A

Olsson, P.-I., Dahlin, T., Fiandaca, G., Auken, E., 2015. Measuring time-domain spectral induced polarization in the on-time: decreasing acquisition time and increasing signal-to-noise ratio. Journal of Applied Geophysics. doi:10.1016/j.jappgeo.2015.08.009

Measuring time-domain spectral induced polarization in the on-time: decreasing acquisition time and increasing signal-to-noise ratio

CrossMark

Per-Ivar Olsson [a,*], Torleif Dahlin [a], Gianluca Fiandaca [b], Esben Auken [b]

[a] Engineering Geology, Lund University, Sweden
[b] Department of Geosciences, Aarhus University, Denmark

ABSTRACT

Combined resistivity and time-domain direct current induced polarization (DCIP) measurements are traditionally carried out with a 50% duty cycle current waveform, taking the resistivity measurements during the on-time and the IP measurements during the off-time. One drawback with this method is that only half of the acquisition time is available for resistivity and IP measurements, respectively. In this paper, this limitation is solved by using a current injection with 100% duty cycle and also taking the IP measurements in the on-time. With numerical modelling of current waveforms with 50% and 100% duty cycles we show that the waveforms have comparable sensitivity for the spectral Cole–Cole parameters and that signal level is increased up to a factor of 2 if the 100% duty cycle waveform is used. The inversion of field data acquired with both waveforms confirms the modelling results and shows that it is possible to retrieve similar inversion models with either of the waveforms when inverting for the spectral Cole–Cole parameters with the waveform of the injected current included in the forward computations. Consequently, our results show that on-time measurements of IP can reduce the acquisition time by up to 50% and increase the signal-to-noise ratio by up to 100% almost without information loss. Our findings can contribute and have a large impact for DCIP surveys in general and especially for surveys where time and reliable data quality are important factors. Specifically, the findings are of value for DCIP surveys conducted in urban areas where anthropogenic noise is an issue and the heterogeneous subsurface demands time-consuming 3D acquisitions.

© 2015 Elsevier B.V. All rights reserved.

1. Introduction

Combined direct current (DC) resistivity and time-domain (TD) induced polarization (IP) measurements are traditionally carried out using a 50% duty cycle waveform for current injection, taking the resistivity measurements during the on-time and the IP measurements during the off-time. Recently, however, developments in time-domain hardware have made it possible to perform detailed monitoring and analysis of the measuring procedure of DCIP acquisition. As a result of this development, it has been suggested that a 100% duty cycle waveform could be used in time-domain IP, with the IP (spectral) information retrieved from the on-time (Dahlin and Leroux 2010). Furthermore, in frequency-domain, a 100% duty cycle waveform has been successfully used for measuring IP, although retrieving limited spectral information (Zonge et al. 2005, Zonge et al. 1972).

Alongside the hardware improvement, a corresponding development on the software side has taken place. Inversion algorithms that use the current waveform and the full IP decays for extracting the

spectral IP content from TD data have been proposed (Fiandaca et al. 2012, 2013), with applications for landfill characterization (Gazoty et al. 2013, Gazoty et al. 2012a, Gazoty et al. 2012b) and for mapping CO2 transport (Doetsch et al. 2015a) and permafrost seasonal variations (Doetsch et al. 2015b).

For these applications, as well as for others, the use of a 100% duty cycle waveform for DCIP measurements will have substantial advantages compared with the traditionally used 50% duty cycle regarding acquisition time efficiency and signal level. These benefits are highly relevant for the applied DCIP surveys conducted by commercial companies where time and reliable data quality are important factors. In addition, DCIP surveys conducted in urban areas where anthropogenic noise sources are present and the heterogeneous subsurface demands time-consuming 3D acquisitions will have extra benefit from the 100% duty cycle waveform and on-time measurements of IP. To date, it has not been shown whether the 100% duty cycle waveform can be successfully used in TDIP measurements, nor if spectral information can be retrieved in the inversion.

This paper demonstrates that the use of a 100% duty cycle waveform and on-time measurements of the spectral IP information is possible for both synthetic and field DCIP cases. The aforementioned hardware and software developments are used for comparing 50% and 100% duty

---

* Corresponding author at: Teknisk Geologi, Lunds Tekniska Högskola, P.O. Box 118, SE-22100 Lund, Sweden.
  E-mail address: per-ivar.olsson@tg.lth.se (P.-I. Olsson).

cycle waveforms, both in terms of IP spectral information and signal to noise ratio. Section 2 introduces the 100% duty cycle waveform in details, followed by sections presenting results and discussion on the synthetic modelling and a field comparison. The paper ends with a brief conclusion.

2. 100% duty cycle

A step-response for an exemplary homogenous half-space Cole–Cole model was generated with the spectral forward response and inversion code Aarhusinv (Auken et al. 2014) and used for creating synthetic full-waveform data of the 50% and 100% duty cycle waveforms (Fig. 1) by the principle of superposition (Fiandaca et al. 2012).

It can be noted that for the 50% duty cycle waveform with IP measurements during the off-time, the measured IP response decays with time, while for the 100% duty cycle waveform with IP measurements during the on-time, the potential increases during the acquisition. For an easier comparison between the 50% and 100% signals, this paper uses the $V_{DC(j)}$ value (retrieved from a time period at the end of each pulse j) for defining the 100% IP decay for pulse j, $V_{IP100\%(j)}$, as the difference between the $V_{DC(j)}$ value and the measured IP response $V_{response(j)}$ (Eq. (1)):

$$V_{\text{IP100\%}(j)} = V_{\text{DC}(j)} - V_{\text{response}(j)}. \tag{1}$$

The individual 100% IP decays derived with Eq. (1), $V_{IP100\%(j)}$, are averaged according to Eq. (2), making use of the negative or positive sign of the decays:

$$V_{\text{IP100\%,average}} = \frac{1}{n_{\text{pulses}}} \sum_{j=1}^{n_{\text{pulses}}} (-1)^{j+1} \cdot V_{\text{IP100\%}(j)}. \tag{2}$$

For the 50% duty cycle, a normalization of the IP response is traditionally achieved by dividing the IP response potential with the VDC value (VIP/VDC) and presenting the IP response in mV/V (note that this normalization does not define the "normalized chargeability" described for instance by Slater and Lesmes (2002), but is a common unit change). A corresponding normalization for the 100% duty cycle is also suggested in this paper through Eq. (3):

$$V_{\text{IP100\%,normalized}} = \frac{V_{\text{IP100\%,average}} \cdot n_{\text{pulses}}}{V_{\text{DC,average}} \cdot (2 \cdot n_{\text{pulses}} - 1)} \tag{3}$$

where $V_{DC, average}$ represents the DC value averaged over all the pulses in analogy to Eq. (2). The normalization of Eq. (3) differs from the standard IP normalization by the presence of the $\frac{n_{\text{pulses}}}{(2 \cdot n_{\text{pulses}} - 1)}$ factor, which has been introduced in order to facilitate the numerical comparison of 50% and 100% IP duty cycles normalized data.

In fact, as can be seen in Fig. 2A, the magnitude of the chargeability for the 100% duty cycle waveform is initially almost twice the magnitude of the 50% duty cycle waveform if compared without normalization (presented in volt). This doubling is due to the superposition of the off-time IP decay of the 50% duty cycle waveform and the corresponding on-time IP build-up. With the 100% duty cycle waveform, these two responses are superimposed on each other and measured as one. Another way to look at this is to consider that the change in current causing the IP response is doubled when using the 100% duty cycle waveform instead of the 50% waveform for all the pulses except the first, which is initiated from the same current level (i.e. zero ampere, see Fig. 1). Considering that $V_{IP100\%, normalized}$ is computed from the IP responses averaged over all the pulses, the $\frac{n_{\text{pulses}}}{(2 \cdot n_{\text{pulses}} - 1)}$ factor in Eq. (3) standardizes the 100% duty cycle response to the current changes of the 50% duty cycle response.

As a result, with the normalization suggested in this paper (Eq. (3)), expressing the decays in terms of mV/V shows more similar starting and averaged magnitudes for the 50% and 100% IP decays (Fig. 2B). Despite the fact that the normalization proposed in Eq. (3) simplifies the comparison of the 50% and 100% signal levels, the shape of the IP curves differs significantly. In particular, the 100% IP decays defined through Eqs. (1), (2) and (3) are forced to small or negative data values at late times (Fig. 2), depending on the selected integration time for the V_{DC}-value and the last IP gate respectively, even though the corresponding 50% IP responses have not reached their minimum. In this paper, this effect is accounted for by the modelling/inversion software, which includes the current waveform, the definition of the DC integration time and the full IP decays in the computations (Fiandaca et al. 2013, Fiandaca et al. 2012).

When looking at the comparison of non-normalized 100% and 50% duty cycle data a final consideration can be drawn about the signal-to-noise ratio. In fact, the noise in IP data depends on the non-normalized signal level (Gazoty et al. 2013), and the almost doubled signal of the 100% duty cycle data can increase the signal-to-noise ratio by up to 100%.

3. Synthetic modelling

Forward modelling and sensitivity analysis of resistivity and the Cole–Cole parameters for both the 50% and the 100% duty cycle waveforms were carried out on a 1D synthetic model (Fiandaca et al. 2013, Fiandaca et al. 2012). The sensitivity, s, is computed through the covariance of the estimator error for linear mapping described by Tarantola
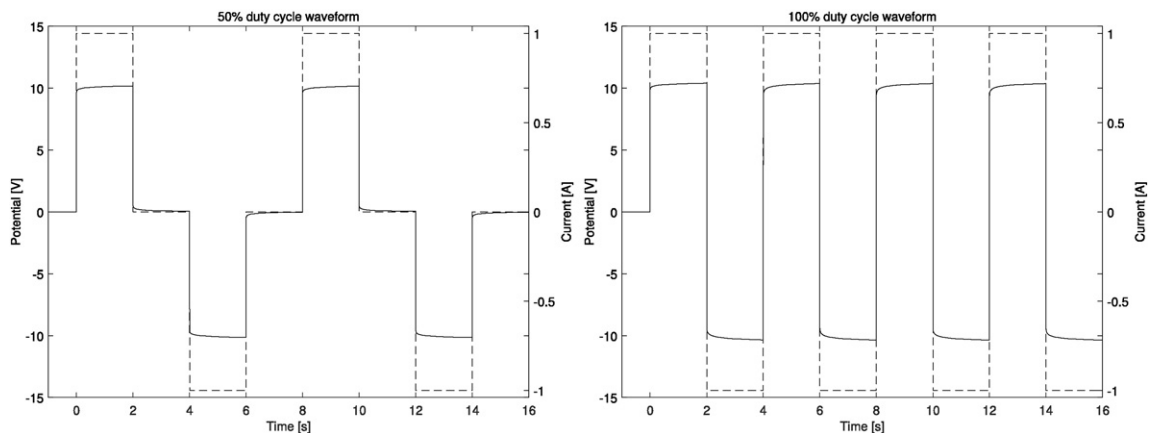

Fig. 1. Modelled waveform for the 50% (A) and 100% (B) duty cycle waveforms showing measured potential (solid line) and injected current (dashed line). Twice as many stacks are achieved with the 100% duty cycle compared with the 50% duty cycle with the same acquisition time.
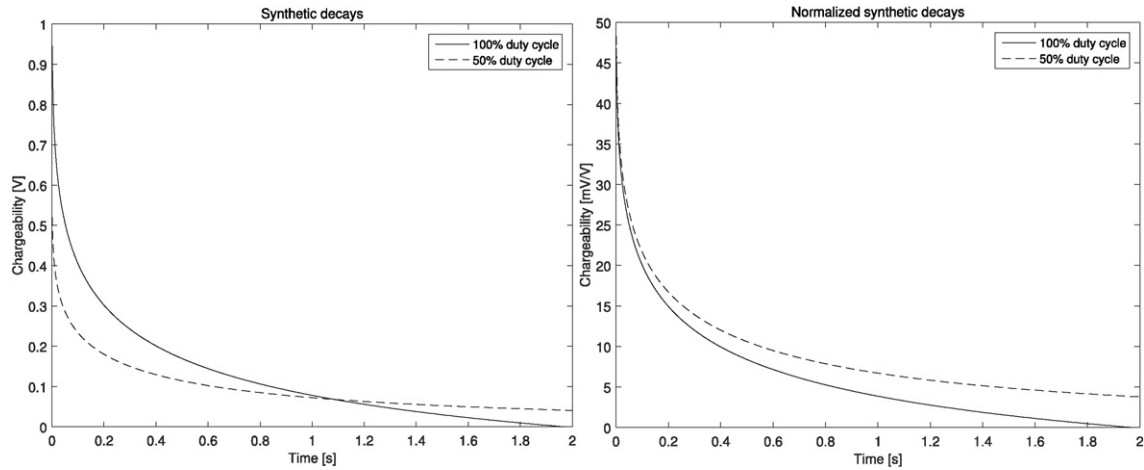
Fig. 2. Modelled IP decays for the 50% (dashed line) and 100% (solid line) duty cycle waveform shown with (B) and without (A) normalization. The normalization of the 100% duty cycle decay was done according to Eq. (3) and $n_{pulses} = 8$, corresponding to the number of modelled pulses (see Fig. 1B). The decays are modelled with Cole–Cole parameters: rho = 50 Ωm, $m_0 = 100$ mV/V, $\tau = 0.5$ s and $C = 0.3$.

and Valette (1982) and represents the relative uncertainty on the model parameters p (because the analysis is performed on the logarithm of the model parameters):

$$p/s \le p \le p \cdot s.$$

A synthetic three layer subsurface model (Table 1), with parameter ranges/contrasts similar to the ones found in the field example described in the next section, was used for the forward modelling of a Schlumberger vertical sounding with log-increasing electrode spacing and IP gate lengths. To emulate field conditions, a noise model identical to the one characterizing the field data was chosen for the sensitivity analysis. In particular, a relative standard deviation of 2% for the DC data and 10% for the IP data were used, together with a voltage dependent noise (Gazoty et al. 2013; Zhou and Dahlin 2003) that better describes the effect of the signal level on the data uncertainty. The voltage dependent noise model was controlled by a nominal voltage noise threshold V_{noise}, defined for a nominal integration time $Nominal_{gatelength}$ and stack size n equal to one, and defined as:

$$\sigma_{DC} = \frac{V_{noise}}{V_{DC}} \cdot \sqrt{\frac{Nominal_{gatelength}}{DC_{gatelength}} \cdot \frac{1}{n}} \quad (4)$$

$$\sigma_{IP} = \frac{V_{noise}}{V_{IP}} \cdot \sqrt{\frac{Nominal_{gatelength}}{IP_{gatelength}} \cdot \frac{1}{n}}. \quad (5)$$

A voltage threshold $V_{noise} = 0.2$ mV with $Nominal_{gatelength} = 0.01$ s was used in the simulations.

The forward modelling and 1D sensitivity analysis was carried out by means of both of the waveforms and four different acquisition cases: two cases with the same on-time ($T_{on} = 4$ s) and amount of stacks ($n = 4$) but with different waveforms (50% and 100% duty cycles) and two other cases where either the on-time either the stacks were doubled for the 100% duty cycle waveform. In theory, the latter two cases give the same total duration of the acquisition as for the 50% duty cycle waveform (Table 2). Table 2 shows that the sensitivity for all

model parameters is comparable for all four acquisition cases, except for the relaxation time of layer two ($\tau - 2$) for which the first (50% duty cycle, $T_{on} = 4$ s, $n = 4$) and that the second last (100% duty cycle, $T_{on} = 8$ s, $n = 4$) cases are more sensitive compared with the others.

4. Field example

The field data were acquired at a farmland with Quaternary deposits of clayey till overlaying a bedrock of Silurian shale. A known dolerite dike intruding the shale provided a chargeable IP structure for the experiment. The DCIP profile (157.5 m, 64 electrodes with a spacing of 2.5 m) was centred on top of the known IP anomaly and retrieved using a multiple gradient array protocol (Dahlin and Zhou 2006) with acid grade stainless steel electrodes and the Abem Terrameter LS instrument. This instrument continuously adapts the output voltage to keep a constant current with an accuracy of 0.4% (Abem 2011), and together with its capability of full-waveform acquisition is particularly well suited for this experiment. Separated cables were used for transmitting current and measuring potentials to reduce the effect of capacitive coupling and improve the IP data quality (Dahlin and Leroux 2012). The electrode contact resistance was measured for all electrodes with a mean value of 220 Ω and a variation coefficient of approximately 45%.

Both the 50% and the 100% duty cycle waveforms were used for DCIP measurements on the field setup. Except for the waveform duty cycle, all other settings were kept equal for the acquisitions: 1015 quadrupoles, 4 s on-time of current injection and 3 full stacks. This resulted in a total acquisition time of 154 min for the 50% duty cycle and 88 min for the 100% duty cycle, a reduction in acquisition time of approximately 43% for the 100% duty cycle waveform. The reason for the reduction not reaching the theoretical 50% (only considering the duration of the waveforms) is that the instrument performs a number of test pulses prior to each current injection. These test pulses are part of the system that enables the instrument to maintain a constant current throughout the injection. In this study, these test pulses were not included in the full waveform modelling.

To get an accurate estimation of the IP response, the background potential variation during a current injection sequence needs to be accounted for. This is also essential for DC resistivity measurement and is commonly handled by measuring and averaging data from a positive–double negative–positive type duty cycle which acts as a filter that removes linear variation (Dahlin 2000), but it should be noted that a higher degree approach may be required in order to recover the more subtle spectral IP information. In this paper, a second order polynomial was adapted to the V_{DC}-values of the stacks and the non-constant terms

Table 1
Layer parameters used for the 1D subsurface model.

Layer	Thickness (m)	ρ (Ωm)	m_0 (mV/V)	τ (s)	c (−)
1	8	250	40	1	0.3
2	14	500	100	2	0.5
3	∞	500	40	1	0.5

Table 2
Sensitivity analysis for both waveforms with same on-time and doubled on-time for the 100% duty cycle. Relaxation time of layer two ($\tau - 2$) for the first and third acquisition cases are indicated with bold font.

Duty cycle	T_{on} (s)	n (—)	$\rho - 1$ (Ωm)	$\rho - 2$ (Ωm)	$\rho - 3$ (Ωm)	$m_0 - 1$ (mV/V)	$m_0 - 2$ (mV/V)	$m_0 - 3$ (mV/V)	$\tau - 1$ (s)	$\tau - 2$ (s)	$\tau - 3$ (s)	$c - 1$ (—)	$c - 2$ (—)	$c - 3$ (—)
50%	4	4	1.015	1.052	1.014	1.40	1.15	1.13	1.54	**1.16**	1.16	1.40	1.12	1.13
100%	4	4	1.015	1.052	1.014	1.47	1.17	1.16	1.54	1.27	1.17	1.47	1.14	1.16
100%	8	4	1.014	1.051	1.014	1.39	1.14	1.12	1.58	**1.14**	1.18	1.39	1.11	1.12
100%	4	8	1.015	1.052	1.014	1.47	1.17	1.16	1.54	1.27	1.16	1.47	1.14	1.15

of this polynomial was used to correct the full waveform recording of measured potential.

Fig. 3 shows field data for both waveforms as apparent resistivity (Fig. 3A and C) and apparent chargeability (IP gate number 5, Fig. 3B and D) pseudosections. The resistivity data show comparable, in terms of spatial distribution and apparent resistivity values, pseudosections for both waveforms. The apparent chargeability pseudosections also have similar spatial distribution but the apparent chargeability section for the 100% duty cycle waveform shows slightly lower values than the 50% duty cycle waveform, when expressed as mV/V. The difference in magnitude of the apparent chargeability, which is also visible in the synthetic IP responses (Fig. 2B), can be explained by the different shapes of the 100% duty cycle waveform at late times, as discussed in Section 2.

Inversion of the field data shown in Fig. 3 were preformed for the spectral Cole–Cole parameters using the Aarhusinv code. The inversions were carried out with L1 model weights using the same inversion settings (noise model and vertical/horizontal weights) for both waveforms. This gave a final data misfit of 1.5 and 1.4 for the 50% and 100% duty cycle data respectively, when using a relative standard deviation of 2% for the DC data, 10% for the IP data and a voltage noise threshold of 0.2 mV.

Fig. 4 shows that the inversion models for the field data acquired with the two waveforms have comparable values for all model parameters and similar data misfit. The geometry of the parameter value distribution in the final inversion models is quite simple but the performance of the 50% and 100% duty cycle waveforms is expected to be comparable also when applied at environments with a more complex subsurface geometry. Similarly, are the performance of the waveforms expected to be comparable also in noiseier field conditions or possibly have better performance with the 100% duty cycle waveform due to higher signal-to-noise ratio? (See Section 2).

Fig. 5 shows the data fit for the quadrupoles with lateral focus (i.e. horizontal position of median sensitivity) corresponding to the middle of the profile (Fig. 4). Similar to what is shown by the synthetic decays (Fig. 2), the acquired field data for the 100% duty cycle waveform are closer to zero for the later gates compared with the 50% duty cycle waveform.

The data acquired from the field tests (Figs. 3 and 5) generally show that the IP decays for the 50% and 100% duty cycle waveforms are different. As discussed above, this difference is in accordance with the synthetic modelling and depends on how the 100% duty cycle IP decay is defined. With an inversion software that includes the injected current waveform and the definitions for the 100% duty cycle IP decay, it is still possible to retrieve an inversion model from the 100% duty cycle data (Fig. 4B) that is similar to the inversion model from the 50% duty cycle waveform data (Fig. 4A).

5. Conclusions

Our results support that the approach of using a 100% duty cycle square waveform for current injection and measuring the IP response during the current on-time is practically applicable. We also show that the measuring time can be substantially reduced by the use of this method and that the signal-to-noise ratio will generally increase.

The results contribute to the usage of commercial IP measurements within areas where the time pressure on projects due to economic constraints is dominant. This is usually the case in engineering and environmental projects but decreasing the total measurement time and improving signal-to-noise ratio are beneficial for all DCIP surveys. Thus, an implementation of a commercial system which makes use of a 100% duty cycle and measures IP during the on-time could have several practical benefits. For example, it may encourage operators to make use of 3D-measurements which generally can be time demanding, to make use of more stacks in noisy environments to get better data quality or to increase the on-time at field sites where long time-constants are expected for the IP decays (such as for example landfills) to get additional spectral information.

The 100% duty cycle and on-time IP measurements described in this paper could be implemented as routine use in DCIP instruments and processing procedures. To actualize this, the instrument used need to
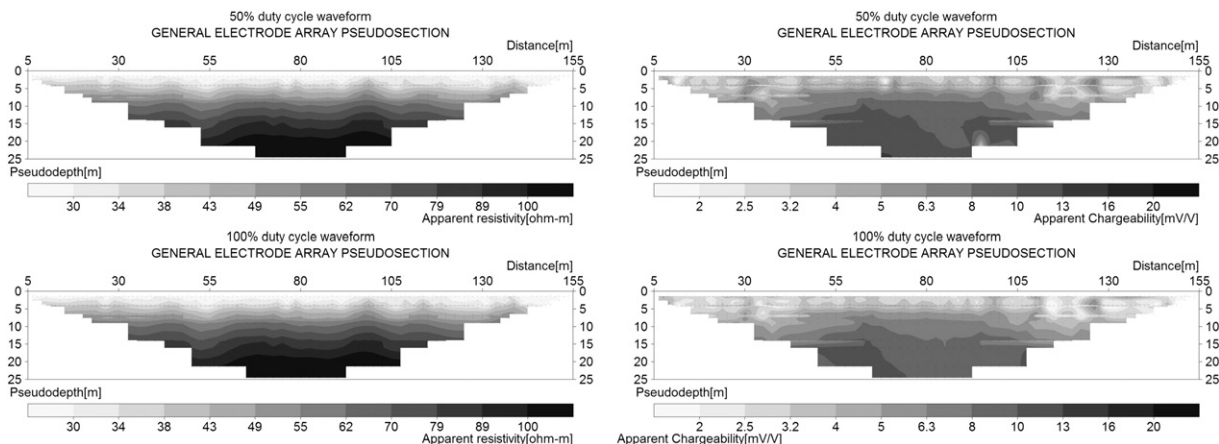

Fig. 3. DC pseudosections (A and C) and IP gate 5 (gate width of 143 ms and centre gate time of 376.5 ms) for the 50% (B) and the 100% (D) duty cycle waveform.
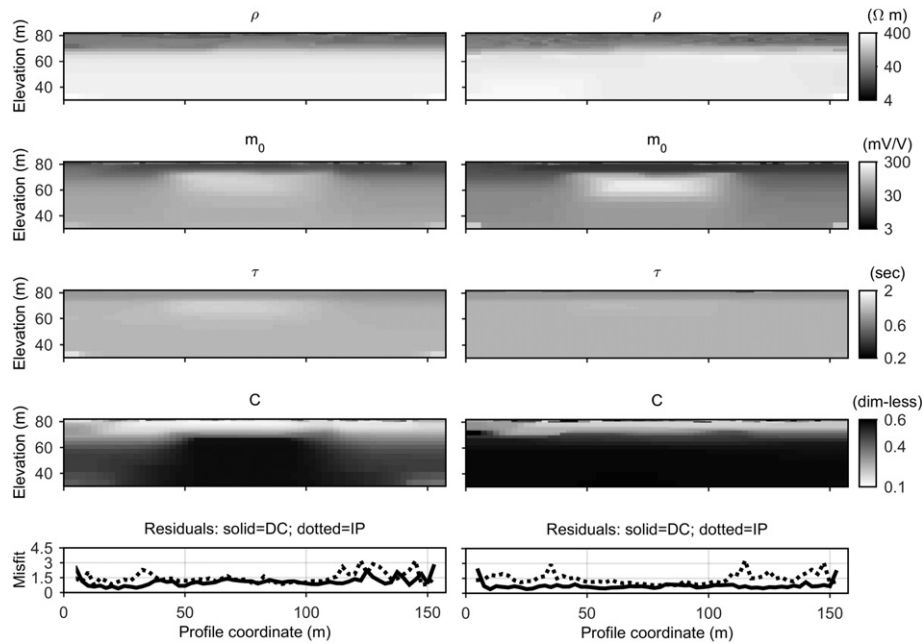
Fig. 4. Inverted sections and data misfit for field data acquired with the 50% (A) and 100% (B) duty cycle waveform.

be able to record full waveform information or be able to gate the data directly during the on-time. The instrument should also be able to keep a stable current waveform. If this is not possible, the waveform of the injected current needs to be fully described in the inversion software and included in the forward computations. These types of inversion software are also advantageous for comparing results from different waveforms (50% duty cycle versus 100% duty cycle).
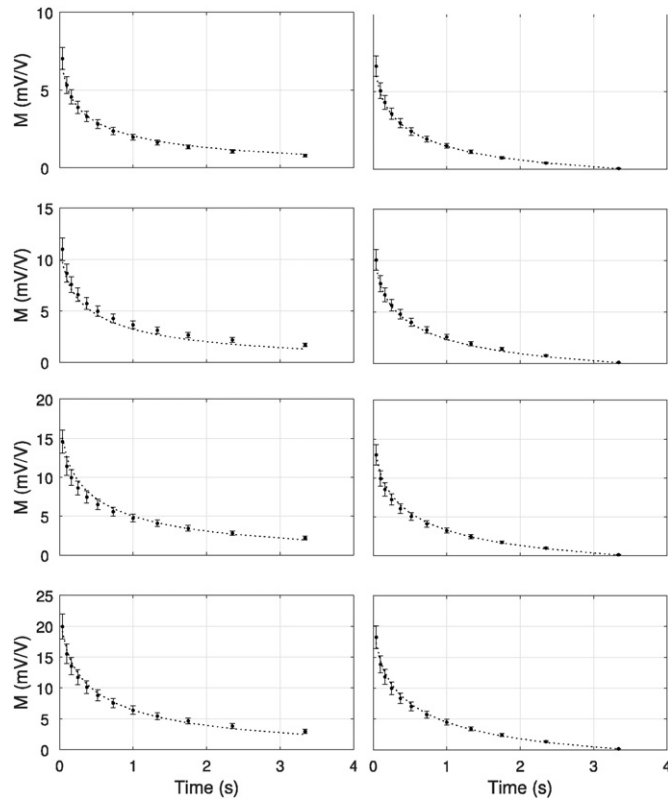

Fig. 5. IP data (points) with error bars (vertical lines) and corresponding forward response (dashed line) for the 50% (A) and 100% (B) duty cycle waveforms. Data shown represents the middle of the field array with increasing pseudo depth from top to bottom.

References

Abem, 2011. Terrameter LS Product Leaflet [www document]. URL http://www.abem.se/support/downloads/technical-specifications/terrameter-ls-leaflet-20111116 (accessed 5.27.14).

Auken, E., Christiansen, A.V., Kirkegaard, C., Fiandaca, G., Schamper, C., Behroozmand, A.A., Binley, A., Nielsen, E., Effersø, F., Christensen, N.B., Sørensen, K., Foged, N., Vignoli, G., 2014. An overview of a highly versatile forward and stable inverse algorithm for airborne, ground-based and borehole electromagnetic and electric data. Explor. Geophys. http://dx.doi.org/10.1071/EG13097.

Dahlin, T., 2000. Short note on electrode charge-up effects in DC resistivity data acquisition using multi-electrode arrays. Geophys. Prospect. 48, 181–187. http://dx.doi.org/10.1046/j.1365-2478.2000.00172.x.

Dahlin, T., Leroux, V., 2010. Full wave form time-domain IP data acquisition, in: 16th European Meeting of Environmental and Engineering Geophysics. doi:http://dx.doi.org/10.3997/2214-4609.20144884

Dahlin, T., Leroux, V., 2012. Improvement in time-domain induced polarization data quality with multi-electrode systems by separating current and potential cables. Near Surf. Geophys. 10, 545–656. http://dx.doi.org/10.3997/1873-0604.2012028.

Dahlin, T., Zhou, B., 2006. Multiple-gradient array measurements for multichannel 2D resistivity imaging. Near Surf. Geophys. 4, 113–123. http://dx.doi.org/10.3997/1873-0604.2005037.

Doetsch, J., Fiandaca, G., Auken, E., Christiansen, A.V., Cahill, A.G., 2015a. Field-scale time-domain spectral induced polarization monitoring of geochemical changes induced by injected CO_2 in a shallow aquifer. Geophysics 16, 10294. http://dx.doi.org/10.1190/geo2014-0315.1.

Doetsch, J., Ingeman-Nielsen, T., Christiansen, A.V., Fiandaca, G., Auken, E., Elberling, B., 2015b. Direct current (DC) resistivity and induced polarization (IP) monitoring of active layer dynamics at high temporal resolution. Cold Reg. Sci. Technol. http://dx.doi.org/10.1016/j.coldregions.2015.07.002.

Fiandaca, G., Auken, E., Christiansen, A.V., Gazoty, A., 2012. Time-domain-induced polarization: full-decay forward modeling and 1D laterally constrained inversion of Cole–Cole parameters. Geophysics 77, E213–E225. http://dx.doi.org/10.1190/geo2011-0217.1.

Fiandaca, G., Ramm, J., Binley, A., Gazoty, A., Christiansen, A.V., Auken, E., 2013. Resolving spectral information from time domain induced polarization data through 2-D inversion. Geophys. J. Int. 192, 631–646. http://dx.doi.org/10.1093/gji/ggs060.

Gazoty, A., Fiandaca, G., Pedersen, J., Auken, E., Christiansen, A. V, 2012a. Mapping of land-fills using time-domain spectral induced polarization data: the Eskelund case study. Near Surf. Geophys. 10, 575–586. doi:http://dx.doi.org/10.3997/1873-0604.2012046

Gazoty, A., Fiandaca, G., Pedersen, J., Auken, E., Christiansen, A. V, 2013. Data repeatability and acquisition techniques for time-domain spectral induced polarization. Near Surf. Geophys. 391–406. doi:http://dx.doi.org/10.3997/1873-0604.2013013

Gazoty, A., Fiandaca, G., Pedersen, J., Auken, E., Christiansen, A.V., Pedersen, J.K., 2012b. Application of time domain induced polarization to the mapping of lithotypes in a landfill site. Hydrol. Earth Syst. Sci. 16, 1793–1804. http://dx.doi.org/10.5194/hess-16-1793-2012.

Slater, L.D., Lesmes, D., 2002. IP interpretation in environmental investigations. Geophysics 67, 77. http://dx.doi.org/10.1190/1.1451353.

Tarantola, A., Valette, B., 1982. Generalized nonlinear inverse problems solved using the least squares criterion. Rev. Geophys. http://dx.doi.org/10.1029/RG020i002p00219.

Zhou, B., Dahlin, T., 2003. Properties and effects of measurement errors on 2D resistivity imaging surveying. Near Surf. Geophys. 1, 105–117. http://dx.doi.org/10.3997/1873-0604.2003001.

Zonge, K.L., Sauck, W.A., Sumner, J.S., 1972. Comparison of time, frequency, and phase measurements in induced polarization*. Geophys. Prospect. 20, 626–648. http://dx.doi.org/10.1111/j.1365-2478.1972.tb00658.x.

Zonge, K.L., Wynn, J., Urquhart, S., 2005. 9. Resistivity, induced polarization, and complex resistivity. Near-surface Geophysics, pp. 265–300 http://dx.doi.org/10.1190/1.9781560801719.ch9.

8.2 Paper B

Olsson, P.-I., Fiandaca, G., Dahlin, T., Auken, E., 2015. Impact of Time-domain IP Pulse Length on Measured Data and Inverted Models, in: Near Surface Geoscience 2015 - 21st European Meeting of Environmental and Engineering Geophysics. doi:10.3997/2214-4609.201413755

Tu 21P2 23
Impact of Time-domain IP Pulse Length on Measured Data and Inverted Models

P.-I. Olsson* (Lund University), G. Fiandaca (Aarhus University), T. Dahlin (Lund University) & E. Auken (Aarhus University)

SUMMARY

The duration of time domain (TD) induced polarization (IP) current injections has significant impact on the acquired IP data as well as on the inversion models, if the standard evaluation procedure is followed. However, it is still possible to retrieve similar inversion models if the waveform of the injected current and the IP response waveform are included in the inversion. The on-time also generally affects the signal-to-noise ratio (SNR) where an increased on-time gives higher SNR for the IP data.

Introduction

Direct current resistivity and time domain induced polarization (DCIP) is a versatile geophysical method which has been developed for over 100 years. Alongside with this development, the use and understanding of time domain induced polarisation (TDIP) have increased in academia as well as in the engineering industry. Some aspects of the TDIP are however generally neglected when conducting DCIP surveys for engineering applications. Specifically, the effect of varying duration of the current injections and the duration of the IP decays are normally not accounted for in the standard procedures. Furthermore, to the knowledge of the authors, there has up to date been only few studies on how the duration of the injected current affects the results retrieved from TDIP measurements (with notable exception of Gazoty et al., 2013).

In this paper we show that the duration of current injections in fact has significant impact on the acquired induced polarization data as well as on the inversion models, if the standard evaluation procedure is followed. The commonly applied inversion of the induced polarization data is only considering the integral chargeability, without taking the waveform of the injected current or the waveform of the IP response into account. Our results show that, with these full waveform considerations included in the inversion, it is possible to retrieve similar inversion models for the induced polarization, independent of the on-time duration. Our results also show that the signal-to-noise ratio (SNR) for the IP information increases with increasing duration of the current injections.

Methods

A field test was conducted using an ABEM Terrameter LS for transmitting current and measuring potentials. Four field data sets were acquired on the same measurement line, using a 50% duty cycle current injection waveform with different on-time and off-time durations: half second, on second, two seconds and four seconds. The retrieved IP decays were gated with approximately log-increasing IP-gates with the same temporal distribution, but with larger number of gates for the longer on-time acquisitions. All other data acquisition parameters were identical. The field data were inverted for resistivity, integral chargeability (Res2dinv) and phase shift (Aarhusinv).

For simplicity, and in order to compare the same amount of parameters for both inversion methods, the constant phase angle (CPA) model was used for the Aarhusinv inversions (Fiandaca et al., 2013, 2012). This model contains only two parameters, in contrast to the more general Cole-Cole model which contains four parameters.

Results and Discussion

Figure 1 shows acquired field IP decays for the same quadruple from the four different on-time data sets. As seen in Figure 1, the starting values of the measured IP decays are increasing with increasing on-time. Furthermore, the magnitudes of the longer on-time decays are higher than for the shorter on-times for the full length of the decays. One direct effect of this is, assuming that noise levels are independent of on-time, is an increase in SNR with increasing on-time.

Figure 1 A*cquired field IP decays corresponding to the same quadruple from each of the four data sets with different on-time. Note that the magnitude of the decays are increasing with longer on-time.*
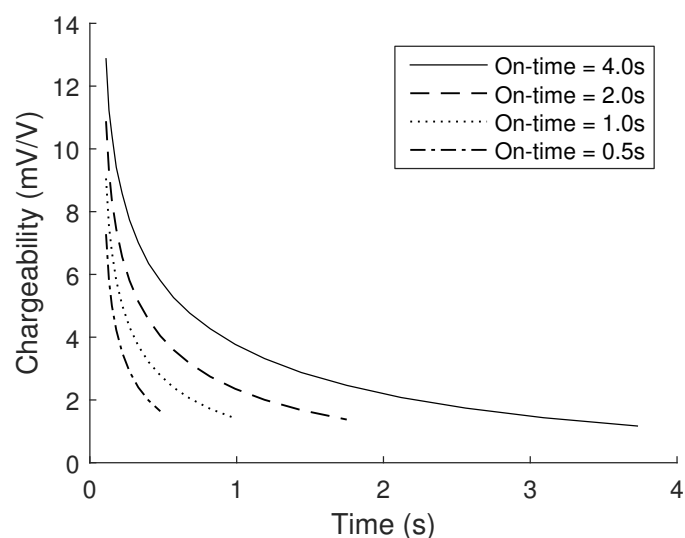
Figure 2 shows pseudosections of apparent chargeability for the 3rd IP-window for three data sets with different on-time. Clearly data space is different for the three data sets even if they were acquired on the same measurement line. More specific, is the apparent chargeability generally increasing when on-time is increased, which is also shown by the individual full decays in Figure 1. One effect of this difference in data space is that inversions not considering the full waveform will produce different inversion models for data acquired with different on-time. Since not only decay duration but also magnitude is different it is not enough to only fix the integration time to for example the Newmont polarization standard (Van Voorhis et al., 1973; Zonge et al., 1972), but full waveform inversion is needed.
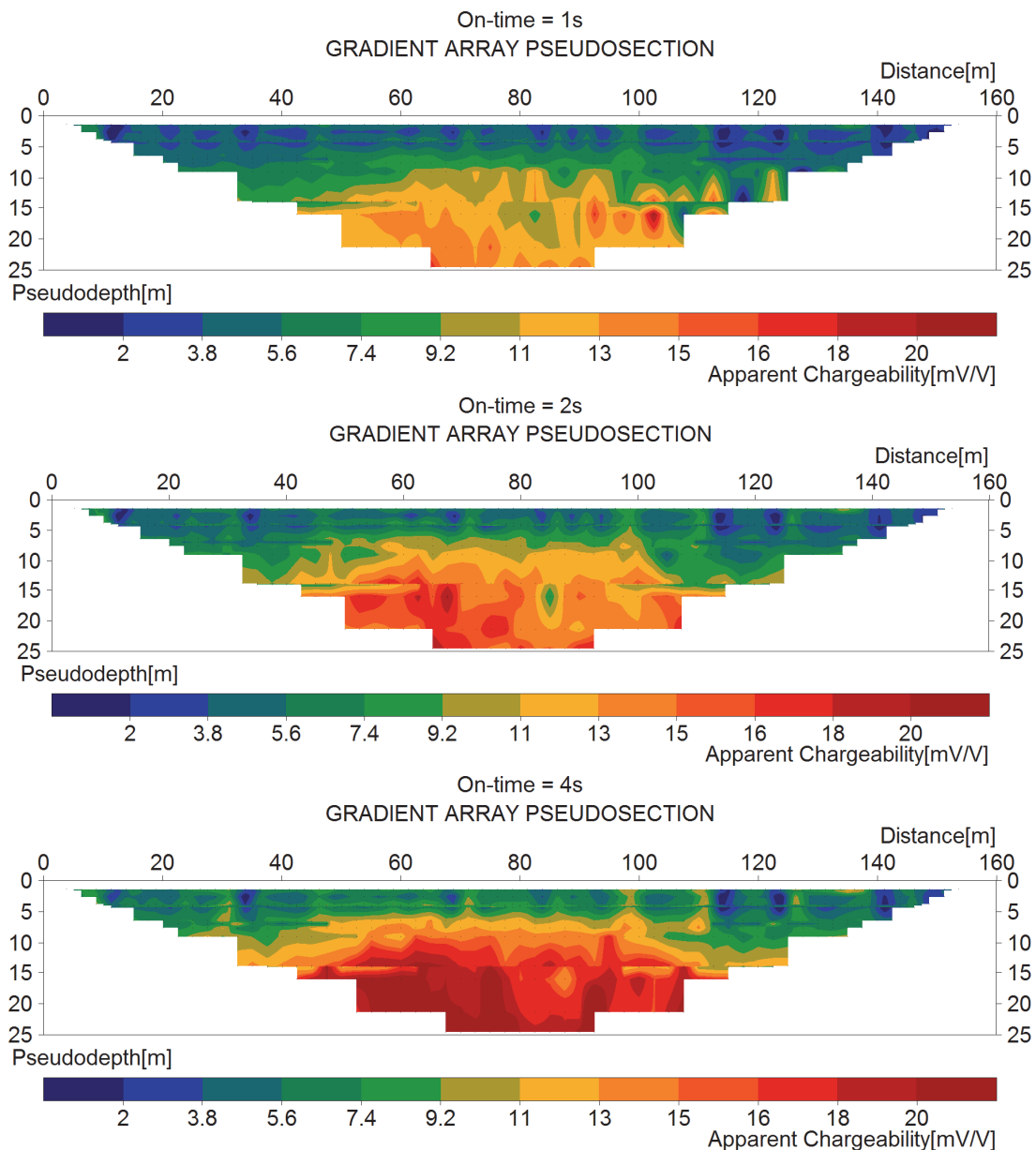
Figure 2 *Pseudosections for apparent chargeability (3rd IP-window) of three different field data sets (on-time=1, 2 and 4 seconds). As seen in the figure is the magnitude of the apparent chargeability increasing with increasing on-time (from top to bottom). This effect can also be seen in the full decays shown in Figure 1.*

Figure 3 shows inversion models retrieved with Res2dinv and Aarhusinv for three data sets acquired on the same measurement line but with different on-time. The resistivity sections are similar for all data sets independent on inversion software. However, as expected when considering the difference in data space, the chargeability models retrieved from the integral chargeability inversions are quite different (Figure 3, 2nd profile from top). On the contrary, more similar inversion models are retrieved when inverting for the CPA-model and taking the waveform of the injected current into account (Figure 3, bottom profile).
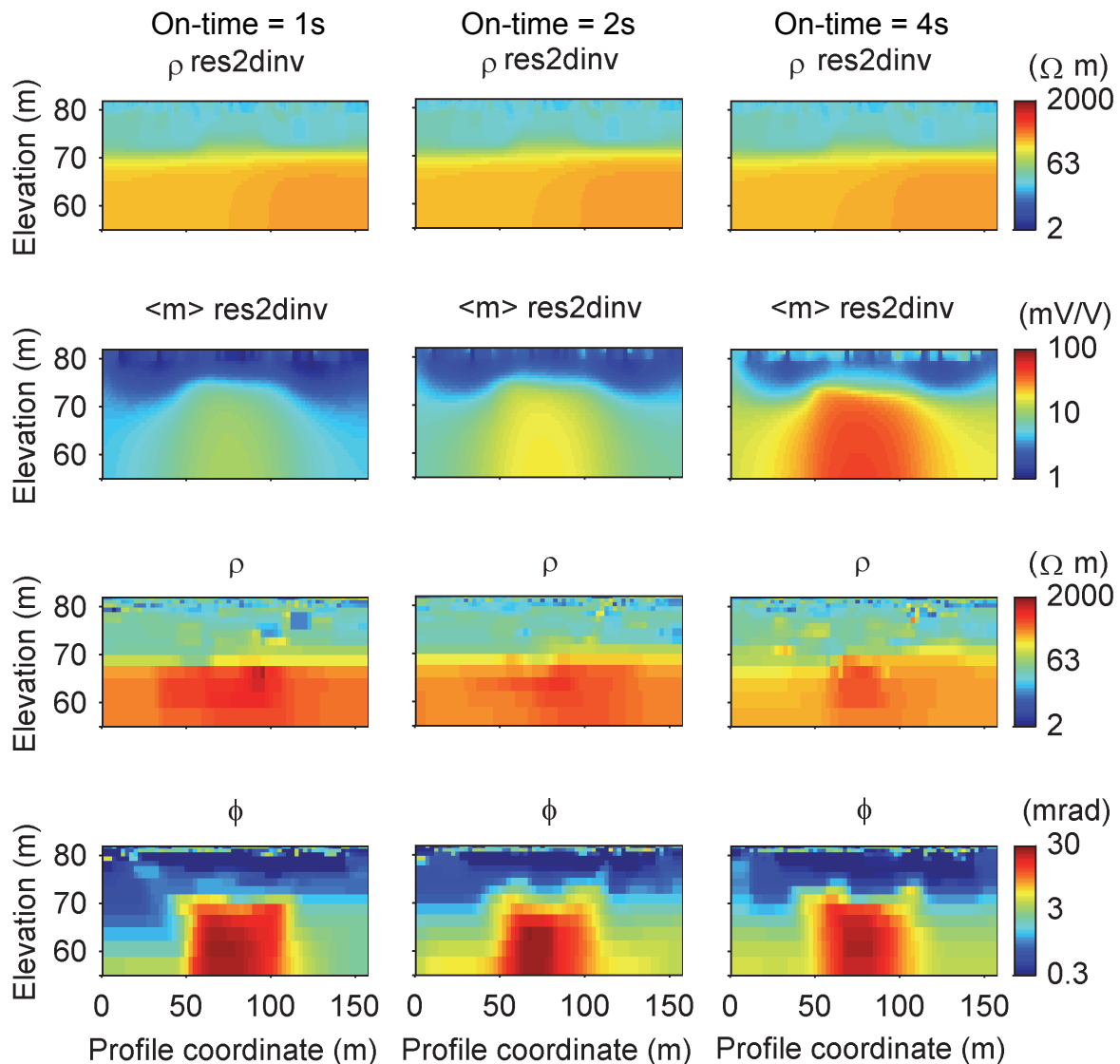
Figure 3 *Inversion models of field data from the same measurement line but with different on-time/off-time. Sections shown are (from top to bottom): resistivity (Res2dinv), integral chargeability (Res2dinv), resistivity (Aarhusinv) and CPA phase shift (Aarhusinv). Clearly, the resulting inversion models for integral chargeability are very different from each other even if they represent inversion of data acquired on the same profile. In contrast, similar inversion models are retrieved when inverting for phase shift and including the waveform of the injected current in the inversion.*

Conclusion

Our results show, that the on-time of the injected current has a substantial effect on retrieved induced polarization field data. It is clear from the results that this difference in data also effects the inverted subsurface IP models when using an inversion software that only considers integral chargeability. However, we have also shown that it is in fact possible to retrieve similar inversion models if the waveform of the injected current and the IP response waveform are included in the inversion and that increasing on-time gives higher SNR for the IP data.

Only considering the integral chargeability can be misleading and likely makes it more ambiguous when trying to relate the IP models to geology building tabular reference data. Furthermore, if not including the full waveform in the inversion, care need to be taken that the same acquisition settings are used when making complimentary or verification measurements so that different data sets will be comparable in data and model space.

Acknowledgements

References

Fiandaca, G., Auken, E., Christiansen, A.V. and Gazoty, A. [2012] Time-domain-induced polarization: Full-decay forward modeling and 1D laterally constrained inversion of Cole-Cole parameters. *Geophysics*, **77**, E213-E225. doi:10.1190/geo2011-0217.1.

Fiandaca, G., Ramm, J., Binley, A., Gazoty, A., Christiansen, A.V. and Auken, E. [2013] Resolving spectral information from time domain induced polarization data through 2-D inversion. *Geophysical Journal International*, **192**, 631-646. doi:10.1093/gji/ggs060.

Gazoty, A., Fiandaca, G., Pedersen, J., Auken, E., Christiansen, A.V. [2013] Data repeatability and acquisition techniques for time-domain spectral induced polarization. *Near Surface Geophysics*, 391-406. doi:10.3997/1873-0604.2013013.

Van Voorhis, G.D., Nelson, P.H., Drake, T.L. [1973] Complex Resistivity Spectra of Porphyry Copper Mineralization. *Geophysics*, **38**, 49. doi:10.1190/1.1440333.

Zonge, K.L., Sauck, W.A., Sumner, J.S. [1972] Comparison of Time, Frequency, and Phase Measurements in Induced Polarization*. *Geophysical Prospecting*, **20**, 626-648. doi:10.1111/j.1365-2478.1972.tb00658.x.

8.3 Paper C

Olsson, P.-I., Fiandaca, G., Larsen, J.J., Dahlin, T., Auken, E., 2016. Doubling the spectrum of time-domain induced polarization: removal of non-linear self-potential drift, harmonic noise and spikes, tapered gating, and uncertainty estimation. to be submitted for publication (Geophysical Journal International).

Title

Doubling the spectrum of time-domain induced polarization: removal of non-linear self-potential drift, harmonic noise and spikes, tapered gating, and uncertainty estimation

Authors and affiliations

Per-Ivar Olsson[1], per-ivar.olsson@tg.lth.se

Gianluca Fiandaca[2], gianluca.fiandaca@geo.au.dk

Jakob Juul Larsen[3], jjl@eng.au.dk

Torleif Dahlin[1], torleif.dahlin@tg.lth.se

Esben Auken[2], esben.auken@geo.au.dk

[1]Engineering Geology, Lund University, Sweden

[2]Department of Geoscience, Aarhus University, Denmark

[3]Department of Engineering, Aarhus University, Denmark

Section

Marine geosciences and applied geophysics

Abbreviated title

Doubling the spectrum of time-domain induced polarization

Corresponding author

Name: Per-Ivar Olsson

Adress: Teknisk Geologi, Lunds Tekniska Högskola, P.O. Box 118, SE-22100 Lund, Sweden.

E-mail address: per-ivar.olsson@tg.lth.se

Summary

This paper presents an advanced signal processing scheme for time-domain induced polarization (TDIP) full waveform data. The processing scheme includes several steps with an improved induced polarization (IP) response gating design using convolution with tapered windows to suppress high frequency noise, a logarithmic gate width distribution for optimizing IP data quality and an estimate of gating uncertainty. Additional steps include modelling and cancelling of non-linear background drift and harmonic noise and a technique for efficiently identifying and removing spikes. The cancelling of non-linear background drift is based on a Cole-Cole model which effectively handles current induced electrode polarization drift, a drift type common in field TDIP measurements. The model-based cancelling of harmonic noise reconstructs the harmonic noise as a sum of harmonic signals with a common fundamental frequency. After segmentation of the full waveform potential and determining of the harmonic noise model parameters for each segment, a full harmonic noise model is constructed and subtracted. Furthermore, the uncertainty of the background drift removal is estimated which together with the gating uncertainty estimate and a uniform uncertainty gives a total, data-driven, error estimate for each IP gate. The processing steps is successfully applied on authentic full field profile data sets acquired in environments with different sources of noise. With the model-based cancelling of harmonic noise, the first usable IP gate is moved one decade closer to time zero. Furthermore, with a Cole-Cole background drift model the shape of the response at late times is accurately retrieved. In total, this processing scheme achieves almost four decades in time and thus doubles the available spectral information content of the IP responses compared to the traditional processing.

Introduction

Recently, the interpretation and inversion of time-domain induced polarization (TDIP) data has changed. Research is moving from only inverting for the integral changeability to also consider the spectral information and inverting for the full induced polarization (IP) response curves. Several examples of spectral TDIP applications for different purposes have been presented (Auken et al., 2014; Doetsch et al., 2015; Gazoty et al., 2013, 2012; Johansson et al., 2015). Furthermore, efforts have been made to achieve faster acquisitions and better signal-to-noise ratio (SNR) by using a 100% duty cycle current waveform, without current off-time, for TDIP measurements (Olsson et al., 2015). However, there still remains drawbacks for the spectral TDIP measurements, especially its limited spectral information content compared to for example laboratory frequency-domain spectral IP measurements (Revil et al., 2015). To date, only limited work has been done on increasing the spectral information content in TDIP measurement data even though recent developments in TDIP acquisition equipment have enabled access to full waveform recordings of measured potentials and transmitted current (e.g. the Terrameter LS and the Elrec Pro). This paper presents a full waveform processing scheme for handling multiple issues limiting the spectral information content. These issues are handled separately starting with background drift removal which is followed by identifying spikes, harmonic denoising, spike removal, tapered gating and uncertainty estimation.

Background drift in TDIP data can have multiple origins, for example: natural potential difference in the subsurface, electrochemical electrode polarization (if not using non-polarizable electrodes) and current-induced electrode polarization (if using same electrodes for injecting current and measuring potentials). The current-induced electrode polarization drift can be orders of magnitude larger than the signal (Dahlin, 2000), thus it is crucial to compensate for this background drift to accurately retrieve the shape of the IP response and be able to extract the spectral IP information from TDIP measurement of the subsurface. The drift is traditionally corrected with a linear approximation (Dahlin et al., 2002; Peter-Borie et al., 2011) which for DC and integral chargeability measurements often can be good enough but when evaluating the spectral IP information a more accurate approximation is needed. This paper presents an improved background drift estimation method using a Cole-Cole model. This model is known to accurately describe polarization effects and is capable of handling both linear (with long Cole-Cole time constants) and more complex non-linear drift cases such as the current-induced electrode polarization.

Spikes originating from anthropogenic sources such as electric fences for livestock management can be registered by TDIP measurements. These spikes can cause problems when extracting IP information, and especially spectral IP from measured field data. For conducting more advanced signal processing of the measured TDIP data it is also important to locate the spikes. This paper presents a novel and efficient processing scheme for enhancing and identifying the spikes with a series of filters on the raw potential signal and by implementing a flexible and data-driven threshold with the use of a Hampel filter (Davies and Gather, 1993; Pearson, 2002).

Harmonic noise originates from the power supply sources oscillating at a base frequency (e.g. 50 Hz or 60 Hz) and harmonics of this base frequency. In TDIP processing today, this is handled by introducing hardware low-pass filters in the instruments and/or with rectangular gating over full period(s) of the known base frequency (e.g. 1/50 s or 1/60 s) for suppressing household power supply frequencies at 50 or 60 Hz and its harmonics. However, the use of low pass filters or long gates causes a loss of early IP response information close to current pulse change and thus makes it more difficult to resolve spectral IP parameters. This is especially severe when the field

measurements are conducted close to electric railways in some countries (e.g. Austria, Germany, Norway, Sweden, Switzerland and USA) where the frequency of the power supply for the trains is even lower (16 ⅔ Hz or 25 Hz) which requires longer gates to suppress the harmonic noise. For the first time in TDIP, a well-known method for cancelling the harmonic noise in data from other geophysical methods (Butler and Russell, 2003, 1993; Larsen et al., 2013; Saucier et al., 2006) is successfully applied on full waveform data. This method models and subtracts the harmonic noise from raw full waveform potential data. Hence, it is possible to use gate widths that are shorter than the time period of the harmonic noise. The shorter gates in turn enable access to much earlier information of the IP response and significantly increase the spectral information by gaining gates one decade in time closer to the current pulse.

Data acquisition: full waveform, sampling rate and aliasing
To be able to apply the processing scheme described in this paper it is necessary to use an instrument that is capable of recording full waveform data of the measured potentials. The required sampling rate for the full waveform depends mainly on the desired width of the shortest gate and how close it should be to the current switch. Another consideration which is related to the input and filter characteristics of the instrument is that the sampling rate need to be sufficiently high to avoid any aliasing problem. The data presented in this paper were acquired with a 50% duty cycle current waveform and 4s on-time using an Terrameter LS instrument for transmitting current and measuring potentials. The instrument operates at a sampling rate of 30 kHz and applies digital filtering and averaging depending on selected data rate (Abem, 2011). A data rate of 3750 Hz, corresponding to approximately 0.267 ms per sample, was used for the measurements presented in the paper. The sampling rate was chosen for being able to have the first IP gate one millisecond from the current pulse, considering that earlier gates would certainly suffer from EM-effects which we at present want to avoid, it was not judged meaningful with earlier gates. The instrument input filters were modified with a 4th order Butterworth filter with cutoff frequency of 1.5 kHz to avoid aliasing.

Two TDIP profiles (74 meter, 38 electrodes with spacing of two meter) were acquired on a grass field in downtown Aarhus, Denmark with presence of multiple noise sources common in urban environments. The profiles were acquired with the instrument and settings as described in the previous paragraph, a multiple gradient protocol (364 quadrupoles) and acid-grade stainless steel electrodes. Full waveform data were recorded for the full profiles and typical examples of raw full waveform potential for one acquisition are shown in Figs 1, 2, 4 to 6, 8 and 9 while the second acquisition is shown as pseudosections in Figure 10. The data example in Fig. 3 was taken from a survey recorded with a similar setup in a rural area in western Denmark using the same instrument and settings.

Redesigned IP gate distribution
For retrieving spectral information close to the current pulses there is a need for gates which are shorter than the time-period of the harmonic noise (i.e. shorter than 20 ms). This is achieved by applying a log-increasing gating scheme that compensates for changes of signal-to-noise ratio throughout the IP response (Gazoty et al., 2013). When the gates are wide enough (i.e. equal to or wider than 20 ms for the 50 Hz harmonic noise) the gate widths are rounded off to multiples of the

time period of the harmonic noise (Table 1, seven gates per decade). Thus, this gate distribution gives access to the IP response information more than one decade closer to the current pulse but still makes use of the efficient noise suppressing gate widths when possible.

Table 1

Figure 1 shows the resulting IP response (green) after gating according to Table 1 and stacking according to the standard procedure (Fiandaca et al., 2012) when using a linear background drift estimate and the IP response retrieved from the instrument (magenta). The re-gated IP response shows similar magnitude as the instrument supplied when the gates are multiples of 20 ms. Contrastingly, it exhibits an erratic behavior until the gate widths are multiples of 20 ms and suppress the 50 Hz harmonic noise. Clearly, the harmonic noise needs to be assessed to enable the use of gates shorter than 20 ms. Furthermore, the tail of both IP responses is increasing at the end as a result of the poor performance of the background drift removal when applying a linear drift model. Thus, to accurately retrieve the shape and spectral content of the IP response it is crucial to improve the drift removal by applying a more flexible drift model.

Figure 1

Signal processing

During TDIP measurements the potential response of the subsurface due to the current injection needs to be determined. However, the potential measured in the field is composed of the sum of multiple, known and unknown, sources (Eq. 1, with sample index *n*). To get an accurate determination of the potential response it is essential to determine and compensate for as many of these sources as possible.

$$u_{measured}(n) = u_{response}(n) + u_{drift}(n) + u_{harmonic\ noise}(n) + u_{spikes}(n) + u_{other}(n)$$

<div align="right">Eq. 1</div>

The known noise sources in Eq. 1 (u_{drift}, u_{spikes} and $u_{harmonic\ noise}$) are handled separately in the processing scheme described in this paper and applied in a sequential manner. The component (u_{other}) represent the effect of all other noise sources (e.g. random noise and quantization error) and is not explicitly handled by the processing scheme even though for example the random noise is reduced by gating the data. The first processing scheme step is the drift removal which is followed by identifying spike samples, harmonic denoising, spike removal, tapered gating and uncertainty estimation according to:

1. Drift removal
2. Identifying and flagging spikes
3. Harmonic noise subtraction
4. Removal of spikes
5. Tapered gating and uncertainty estimation

Given that the processing can accurately remove the background drift, harmonic noise and spikes, the processing output can be described by:

$$u_{processing\ output}(n) \cong u_{response}(n) + u_{other}(n)$$

Eq. 2

thus decreasing the ambiguity of the resulting TDIP data by removing many components of the measured potential which are not representing the IP response (Eq. 2). For continuity, the different parts of the signal processing scheme in this section are presented using one full waveform potential (and current) recording, except for the despiking example (due to lack of spikes in the main full waveform potential data set. The processing scheme is implemented for both 50% and 100% current duty-cycle waveform and is parallelized in the computer software Matlab (2015b) and generally applicable on full profiles as exemplified with the pseudosections in the "Full field profile processing example" section which were acquired for the same profile.

Cole-Cole model-based drift removal

To get an accurate determination of the IP and DC potential, $u_{response}$, from TDIP full waveform data, it is crucial to determine and compensate accordingly for the background drift (Dahlin, 2000; Dahlin et al., 2002). This removal is normally done by approximating the drift as a linear trend (Dahlin et al., 2002; Peter-Borie et al., 2011), even if a more advanced and flexible description of the drift could handle also non-linear cases such as current induced electrode polarization. The current-induced electrode polarization is known to be orders of magnitude larger than the signal (Dahlin, 2000) and is a common issue during field surveys due to difficulties of designing meaningful measurement sequences that account for all recent current injections. Electrode contact tests performed before initiating the TDIP measurements can also be a source for the current induced electrode polarization. The current-induced electrode polarization background drift is caused by a depolarization phenomenon which is known to be well described by the Cole-Cole model (Cole and Cole, 1941) and thus it is especially suitable for estimating the background drift. Three different background drift approximations, summarized in Table 2, are included: the first with a linear estimate, the second with a Cole-Cole estimate and the third with the instrument drift estimate which is also linear but with slightly different implementation.

Table 2

The fitting of the drift model parameters is conducted on an averaged and down-sampled subset of the potential full waveform signal. The averaging window is set to to a full period (e.g. 20 ms for 50 Hz) of the fundamental frequency of the harmonic noise so that these harmonic oscillations are suppressed. Furthermore, to reduce the risk of any IP response interfering with the drift model the fit is conducted for a subset of the down-sampled signal, taken at the end of the off-time period for the 50% duty-cycle (Figure 1) and on-time period if applying a 100% duty-cycle current waveform.

Figure 2 show examples of generated drift models, as well as the resulting IP responses after gating (see Table 1 for gate widths) and stacking the signal. In the drift model and full waveform plot (Figure 2 bottom), there is a relatively large difference between re-gated linear model (green) and the data for model fit (grey x-markers). Clearly, the linear model is not sufficient for accurately

describing the drift in the full waveform potential and as a result it gives unrealistic increasing chargeability values for late gates of the IP response (green line, Figure 2 top). Contrastingly, the Cole-Cole model (blue line, Figure 2 bottom) shows a good fit to drift data and consequently the resulting IP response does not exhibit the erroneous behavior at late gates. In total, it is clear that a linear drift model gives incorrect IP responses, especially at late times when signal-to-noise ratio is smaller and that a more advanced drift model such as the Cole-Cole is needed.

Figure 2

Removal of full waveform spikes
Despiking of the measured full waveform signal is done for two main reasons. The first reason is that spikes in the full waveform data can corrupt the integrated values for IP gates. Since the spikes normally last for a fraction of millisecond, and have average close to zero (bipolar spikes), this problem is uncommon for long gates where all spike samples of an individual spike fall within the gate. However, for short gates consisting of a few samples, often only part of the spike falls within the gate thus having large effect on the integrated value. The second reason for finding the spikes in the full waveform data is related to the modelling of the harmonic noise and how the finding of noise model parameters is implemented in this paper which is known to be sensitive to spikes in data (Dalgaard et al., 2012).

The method for finding the spikes described in this paper uses several steps to enhance the spikes in the signal and defines a data-driven, automatic threshold limit to determine if a sample index (n) is to be considered as spike or not:

1. A simple and efficient first order high pass filter (Eq. 3) is applied on the full-waveform signal ($u_{measured}(n)$, first row in Figure 3) for removing DC offset and enhancing spike visibility:

$$u_2(n) = u_{measured}(n) - u_{measured}(n-1)$$

Eq. 3

2. The spike are further enhanced by applying a non-linear energy operator filter (Eq. 4) on the output from the first step (u_2, second row in Figure 3) and taking the absolute value:

$$u_3(n) = abs(u_2(n)^2 - u_2(n-1) \cdot u_2(n+1))$$

Eq. 4

3. The signal u_3 (black line, third row in Figure 3) is down-sampled by taking the maximum value within 20 ms segments, creating a data-driven threshold variable which accepts all samples.
4. A Hampel filter (Davies and Gather, 1993; Pearson, 2002) is applied on the output from step 3. The Hampel filter computes the median of the sample and its neighbor samples (4 on each side in our examples) and estimates the standard deviation (STD) using mean absolute deviation. If the sample value differs more than 3 STDs from median, the sample value is replaced with the median. Thus, this filter lowers the threshold value for large amplitude changes in the u_3 signal.

5. The output from step 4 is interpolated with 1D linear interpolation for each sample index in u_3.

By applying the Hampel filter in this manner an automatic data-driven threshold variable along the full-waveform acquisition is defined, as shown in Figure 3 (third row, red curve). All the samples above the threshold are marked as spikes (Figure 3, red x-marker) and are neglected performing the calculations for the residual energy in the harmonic denoising procedure.

Figure 3

This routine identifies spikes in the full waveform potential during the on and off-time of the current injections (Figure 3, red x-marker) as well as spikes created by current switches (Figure 3, green x-marker). The current switch spikes are considered as spikes for the succeeding harmonic denoising (see Model-based cancelling of harmonic noise) but neglected when replacing the values of the spike samples. The despiking is done as a last step of the overall signal processing, after the cancelling of harmonic noise, by replacing spike sample values with the median of its 8 neighboring samples (4 on each side) in the processed potential.

Model-based cancelling of harmonic noise

The signal processing approach described in this section is similar to the processing successfully applied on data from other geophysical methods, for example magnetic resonance soundings (Larsen et al., 2013) and seismoelectrics (Butler and Russell, 1993) but it has in this case been adapted to be applicable for data from TDIP measurement. The method takes a model-based approach for processing the TDIP full waveform potential by describing the harmonic noise in terms of a sum of harmonic signals (Eq. 5). The different harmonic signals have frequencies given by a common fundamental frequency (f_0) multiplied with an integer (m) to describe the different harmonics but have independent amplitudes (α_m and β_m) for each harmonic m:

$$u_{harmonic\ noise}(n) = \sum_m \left(\alpha_m \cos\left(2\pi m \frac{f_0}{f_s} n\right) + \beta_m \sin\left(2\pi m \frac{f_0}{f_s} n\right) \right)$$

$$\text{Eq. 5}$$

where α_m and β_m determines amplitudes and phases of a single cosine signal (Larsen et al., 2013). By accurately determining the noise model parameters it is possible to precisely describe the harmonic noise component of the measured potential and to compensate accordingly by subtracting the harmonic noise model from $u_{measured}$

It is necessary to find the values for model parameters f_0, α_m and β_m in Eq. 5. These parameters are however not constant for the time-scale (tens of seconds to minutes depending on acquisition settings) of a TDIP measurement. The frequency can for example vary up to ±0.5 Hz in this time frame (Li et al., 2011). Furthermore, a fundamental frequency estimate which deviates with only some millihertz from the optimal value will reduce the noise cancelling efficiency (Larsen et al., 2013), so a more advanced method is needed for applying the model-based harmonic denoising method on TDIP data. To handle this issue, the raw full waveform potential is divided into shorter segments so that the variation within the segments can be considered small. However, it is not

suitable to use too short segments since enough information is needed to be able to accurately determine the values of the model parameter. Butler and Russell (1993) shows that the error of the estimated model parameters decreases with increasing segment length and also point out that the best estimates of model parameters are achieved when the segment length is a multiple of the period of the fundamental frequency (e.g. 20 ms multiples for f_0=50 Hz). This means that the selection of segment length is a trade-off between a short segment length to make sure that the model parameters are not changing too much and a long segment length to enable an accurate estimate of the parameter values. To compensate for this limitation, the segments of the TDIP signal are allowed to overlap so that it is possible to make dense temporal estimates of the model parameters but still having long enough segments. Experience from processing several different TDIP data sets has shown that a segment length including overlap in the range of 200-300 ms is suitable to achieve good processing results. For the processing in this paper a segment length of 220 ms and overlap of 20 ms was used.

After segmenting the full waveform potential the finding of the noise model parameters is done by minimizing the residual energy $E_{residual}$ after subtracting a temporary harmonic noise model from the recorded full waveform potential segment:

$$E_{residual} = \sum_n (u_{measured}(n) - u_{harmonic\ noise}(n))^2$$

Eq. 6

The minimum residual energy for each segment is determined with an iterative approach using golden section search and parabolic interpolation for minimizing the residual energy by changing the fundamental frequency within a given interval around the expected frequency (e.g. 50 ± 0.5 Hz). For each of the tested frequencies the α_m and β_m parameters are determined using a least-squares routine and a temporary noise model is constructed according to Eq. 5. For processing efficiency, a subset of the harmonics is used for the noise model when determining fundamental frequency. The subset is chosen by taking the mhigh harmonics with the highest estimated power spectral density energy compared to the baseline (green circle marker in Figure 4, mhigh=10) so that harmonics with no or little energy are not modelled. After identifying the fundamental frequency for a segment, the αm and βm parameters are recalculated for all harmonics up to fs/2, i.e. half of the sampling frequency. Finally, the parameters are interpolated by using the values of the nearest segment and a full noise model is calculated for each sample in the potential signal (Figure 5) by evaluating Eq. 5.

Figure 4 shows the estimated power spectral density for a full waveform potential recording before and after applying the harmonic denoising. The original signal (black) exhibits distinct peaks of energy at 50 Hz and integer multiples of this frequency corresponding to the harmonics. In the corresponding energy estimate after the harmonic denoising (red) the energy peaks have been reduced to the baseline energy as a result of modelling and subtracting the harmonic noise. The remaining energy peaks after harmonic denoising (e.g. at approximately 430, 530, 630 and 780 Hz) are not harmonics of the 50 Hz household power supply and thus not removed by the processing. However, these energy peaks can be partially removed by applying a sequential harmonic cancelling with also 16⅔ Hz as fundamental frequency but due to their unknown source(s), the model-based harmonic cancelling might not be applicable and thus these results are not presented in this paper.

Figure 4

Figure 5

Figure 6 shows an example of fully processed full waveform potential, raw full waveform potential and injected current (top). A clear improvement can be seen when comparing the raw full waveform potential with the processed potential, neither the background drift nor the harmonic oscillations are noticeable in the processed full waveform potential. The resulting IP response when including the harmonic denoising in the processing (Figure 6, bottom, blue line) shows a clear improvement compared to the IP response with same processing but without the harmonic denoising (black). The erratic behaviors for early gates is removed and the magnitude of the IP response is gradually decreasing already from the third gate. These improvements extend the first usable spectral IP information to around 2 ms after the current pulse. The first two gates show an unexpected behavior with increasing values also after applying the harmonic denoising, this is due to potential spikes present close to the start of current off-time (black line, Figure 6 top).

Figure 6

Tapered gate design and error estimation
Today, the standard procedure for gating IP is to average the data within the predefined IP gates, corresponding to a discrete and normalized convolution with a rectangular window. In other geophysical methods (e.g. electromagnetic) a gate method applying different kinds of tapered windows have been used since decades (Macnae et al., 1984; Mccracken et al., 1986). One reason for using tapered window functions is that the suppression of high frequency noise is superior compared the rectangular. Furthermore, the tapered windows allow the use of wider gates which has higher noise suppression, without distorting the signal. An example of this effect is seen in Figure 7, comparing a rectangular window with a wider (3.5 times) Gaussian window in time-domain and frequency-domain. In frequency-domain, the main lobe of both windows cuts at approximately the same normalized frequency but the side lobes of the Gaussian have around 40 dB order of magnitude of suppression. This corresponds to an order of two difference in noise suppression, thus the Gaussian window is superior in reducing the noise contribution from higher frequencies compared to the rectangular window.

Figure 7

Uncertainty estimation of the data for individual IP gates cannot be retrieved by directly comparing the individual IP stacks because each individual stack is different due to superposition from previous pulses (Fiandaca et al., 2012), hence other approaches are needed. It is also desirable that an uncertainty estimate make use of the advantage of applying the convolution with tapered gates as described in this paper. If enough gates per decade are used for gating the data, the signal variability is almost linear within the gates and for IP signals the linearity is more evident in lin-

log space. Thus, it is possible to use a linear fit of the convoluted gate in lin-log space for estimating the gate uncertainty by taking the difference between the fit and the convoluted gate data. The difference gives a measure of the noise content within the gate after the convolution. In fact, whenever the noise level is low and enough gates per decade is used (i.e. normally seven to ten), the misfit is negligible. Contrastingly, if random noise or residual harmonic noise is present the gate misfit between the convoluted signal and the linear fit represents a measure of the gating uncertainty. By using the convoluted gate signal for estimating the uncertainty, the measure takes into account the convolution used in the processing.

Figure 8 demonstrates the different steps for estimating the gating uncertainty (STD_{gating}, Eq. 7 and Eq. 9) for each gate using gate number eight as example. As the first step, the full waveform IP gate data processed with Cole-Cole drift removal, despiking and harmonic denoising are stacked according to standard procedure (blue line). After stacking, the processed and stacked data are convoluted with a Gaussian window (3.5 times gate width) of logarithmically increasing window widths for each gate (magenta line). In the next step, a linear fit of convoluted signal is done in lin-log space (green line), since the IP response signal is more linear compared to other log/lin combinations. Next, the integrated IP value for the gate is retrieved by evaluating the linear fit at the log-center of the gate (red x-marker). Lastly, the gating STD on the value (red error bar) is computed as a sum of the misfit between convoluted data and linear fit for all samples ($N_{gate\ samples}$) as follows in Eq. 7:

$$STD_{gating} = \sqrt{\frac{1}{N_{gate\ samples}} \sum_{n=1}^{N_{gate\ samples}} (convoluted\ data(n) - linear\ fit(n))^2}$$

<div align="right">Eq. 7</div>

Figure 8

The uncertainty due to gating the data is not the only possible source of error in the processing. As shown in Figure 2 also the background drift removal can have a large impact on the resulting IP responses and the fit of the drift model gives a useful measure of the remaining drift uncertainty. Similarly to the estimation of gating uncertainty, the drift uncertainty (STD_{drift}) is estimated from the sum of misfit between drift data (grey x-marker in Figure 2) and Cole-Cole drift fit (blue line in Figure 2) for all drift data samples ($N_{drift\ data}$) according to Eq. 8.

$$STD_{drift} = \frac{1}{N_{drift\ data}} \sqrt{\sum_{k=1}^{N_{drift\ data}} (drift\ data(k) - drift\ fit(k))^2}$$

<div align="right">Eq. 8</div>

The total uncertainty (STD_{total}) is computed by summing up the gating, drift and a uniform STD according to Eq. 9.

$$STD_{total} = \sqrt{STD_{gating}^2 + STD_{drift}^2 + STD_{uniform}^2}$$

<div align="right">Eq. 9</div>

Finally, Figure 9 shows the processed IP response in terms of values and relative total STDs with 5% of uniform STD and also the IP response as given by the instrument. The STD error bars increase at early times since the gates are shorter which gives higher STD_{gating} while at late times the drift uncertainty increases and STD_{drift} contributes more to the total gate STD. Note that error bars with the total error captures the fluctuations in data well if the first two gates are disregarded. These two first gates are considered to be artefacts created by the potential spikes at the end of current pulses (Figure 2 and Figure 6). Moreover, the first reliable gate (gate number 3) corresponds to approximately two ms after the current pulse compared to 20 ms for the instrument output. In total with the processing described by this paper, 23 usable gates are achieved giving six new gates at early times corresponding to almost one decade in time and five gates at times where the instrument response presents a bias due to the poor performance of its linear background drift removal.

Full field profile processing example
The processing scheme presented by this paper has been successfully applied to the entire test datasets with substantial improvements in spectral information content, data reliability and quality. One of the datasets is presented here as an illustration. Figure 9 shows IP responses from instrument processing (magenta, instrument output) and the redesigned processing scheme presented by this paper (blue). The spurious IP increase present at late times in the response retrieved by the instrument is removed in the reprocessed IP response as a result of the improved drift removal. At the same time, the harmonic denoising processing enables to retrieve reliable IP data already two ms after the current switch, one decade closer to time zero compared to classic IP processing. Altogether, the proposed processing scheme doubles the spectral content of the reprocessed response compared to the instrument IP processing.

Figure 9

Figure 10 shows pseudosections for a full data set acquired on the same profile as the previous data example (except Figure 3) was extracted from. It shows IP gate 3, 6, 9, 12, 18 and 25 from IP responses generated by the full signal processing routine described by this paper and corresponding pseudosections for the same gates but only applying the linear background drift removal. For the early gates which are not a multiple of the time period of the harmonic noise (gate 3, 6, 9 and 12) there is a clear improvement with much smoother pseudosection from gate 3 (center gate time 2.2 ms) and higher. This suggests that with some minor visual inspection and manual filtering, IP data can be used already 2.2 ms after the current pulse is turned off or changes polarity, thus moving the first gate approximately one decade closer to the pulse compared to the traditional IP processing (10 ms delay time, and a first gate width of 20 ms giving a center gate time of 20 ms). Contrastingly, IP gate number 18 which is a multiple of the time period of the harmonic noise and hence little

affected by the background drift removal (Figure 2 top) shows very similar pseudosections for the two processing examples. However, the pseudosections for the last IP gate (25), which is known to be affected by the applied drift model again show some differences. This difference is due to the sensitivity of the late gates for different background drift estimates where the linear drift model sometimes causes the IP responses to increase at late times. Again, the improved processing with Cole-Cole model drift estimate shows smoother variation in the pseudosection, especially for the left side of the pseudosection.

Figure 10

Conclusion

The TDIP signal processing scheme described in this paper significantly improves the handling of background drift, spikes and harmonic noise superimposed on the potential response in the measured full waveform potential. The Cole-Cole background drift removal substantially increases the accuracy of the drift model for non-linear drift cases and recovers the shape of the IP response at late times with less bias. The reliability of early IP response times, down to a few ms, is generally increased with a flexible data-driven despiking algorithm and model-based harmonic denoising. Furthermore, the improved gate distribution and tapered design gives access to early spectral IP response information and overall increases the signal-to-noise ratio by applying tapered and overlapped gates without distorting the IP response. Additionally, the data driven uncertainty estimates of the individual IP gate values provides valuable information for assessing data quality and for succeeding spectral inversion. In total, this processing moves the first gate one decade closer to time zero, recovers the late gates with reduced bias and supplies valuable estimates of IP gate uncertainty. These improvements double the usable spectral information of the IP response, achieving almost four decades in time, compared to current instrument processing procedure.

Nonetheless, the presented processing scheme includes assumptions and possible problems. The parameters of the harmonic noise model are assumed to be constant within each segment, rapidly varying parameters will not be modelled or compensated. In addition, the background drift models account for smooth varying DC offsets, faster variations (e.g. generated by subways running on DC) are not modelled. On the other hand, processing scheme modules could possibly be upgraded or added to handle also these noise conditions.

The processing scheme presented by this paper has been successfully applied on the test datasets, which originate from both urban and rural field sites, with substantial improvements in spectral information content, data reliability and quality. This development of increase in data reliability and information content is broadening the possibilities and applicability of the spectral TDIP method in the field. Furthermore, it is a promising development for research linking together lab and field measurements and also for extending the use of the method as a standard tool outside the research community.

Acknowledgements

References

Abem, 2011. Terrameter LS Product Leaflet [WWW Document]. URL http://www.abem.se/support/downloads/technical-specifications/terrameter-ls-leaflet-20111116 (accessed 5.27.14).

Auken, E., Doetsch, J., Fiandaca, G., Christiansen, A.V., Gazoty, A., Cahill, A.G., Jakobsen, R., 2014. Imaging subsurface migration of dissolved CO2 in a shallow aquifer using 3-D time-lapse electrical resistivity tomography. Journal of Applied Geophysics 101, 31–41. doi:10.1016/j.jappgeo.2013.11.011

Butler, K.E., Russell, R.D., 1993. Subtraction of powerline harmonics from geophysical records. Geophysics 58, 898. doi:10.1190/1.1443474

Butler, K.E., Russell, R.D., 2003. Cancellation of multiple harmonic noise series in geophysical records. Geophysics 68, 1083–1090. doi:10.1190/1.1581080

Cole, K.S., Cole, R.H., 1941. Dispersion and Absorption in Dielectrics I. Alternating Current Characteristics. The Journal of Chemical Physics 9, 341. doi:10.1063/1.1750906

Dahlin, T., 2000. Short note on electrode charge-up effects in DC resistivity data acquisition using multi-electrode arrays. Geophysical Prospecting 48, 181–187. doi:10.1046/j.1365-2478.2000.00172.x

Dahlin, T., Leroux, V., Nissen, J., 2002. Measuring techniques in induced polarisation imaging. Journal of Applied Geophysics 50, 279–298. doi:10.1016/S0926-9851(02)00148-9

Dalgaard, E., Auken, E., Larsen, J.J., 2012. Adaptive noise cancelling of multichannel magnetic resonance sounding signals. Geophysical Journal International 191, 88–100. doi:10.1111/j.1365-246X.2012.05618.x

Davies, L., Gather, U., 1993. The Identification of Multiple Outliers. Journal of the American Statistical Association 88, 782–792. doi:10.2307/2290763

Doetsch, J., Fiandaca, G., Auken, E., Christiansen, A.V., Cahill, A.G., 2015. Field-scale time-domain spectral induced polarization monitoring of geochemical changes induced by injected CO2 in a shallow aquifer. Geophysics 16, 10294. doi:10.1190/geo2014-0315.1

Fiandaca, G., Auken, E., Christiansen, A.V., Gazoty, A., 2012. Time-domain-induced polarization: Full-decay forward modeling and 1D laterally constrained inversion of Cole-Cole parameters. Geophysics 77, E213–E225. doi:10.1190/geo2011-0217.1

Gazoty, A., Fiandaca, G., Pedersen, J., Auken, E., Christiansen, A. V, 2012. Mapping of landfills using time-domain spectral induced polarization data: The Eskelund case study. Near Surface Geophysics 10, 575–586. doi:10.3997/1873-0604.2012046

Gazoty, A., Fiandaca, G., Pedersen, J., Auken, E., Christiansen, A. V, 2013. Data repeatability and acquisition techniques for time-domain spectral induced polarization. Near Surface Geophysics 391–406. doi:10.3997/1873-0604.2013013

Johansson, S., Fiandaca, G., Dahlin, T., 2015. Influence of non-aqueous phase liquid configuration on induced polarization parameters: Conceptual models applied to a time-domain field case study. Journal of Applied Geophysics. doi:10.1016/j.jappgeo.2015.08.010

Larsen, J.J., Dalgaard, E., Auken, E., 2013. Noise cancelling of MRS signals combining model-based removal of powerline harmonics and multichannel Wiener filtering. Geophysical Journal International 196, 828–836. doi:10.1093/gji/ggt422

Li, Z.W., Samuelsson, O., Garcia-Valle, R., 2011. Frequency deviations and generation scheduling in the nordic system. 2011 IEEE Trondheim PowerTech 1–6. doi:10.1109/PTC.2011.6019176

Macnae, J.C., Lamontagne, Y., West, G.F., 1984. Noise processing techniques for time-domain EM systems. Geophysics 49, 934–948. doi:10.1190/1.1441739

Mccracken, K.G., Oristaglio, M.L., Hohmann, G.W., 1986. Minimization of noise in electromagnetic exploration systems. Geophysics 51, 819–832. doi:10.1190/1.1442134

Olsson, P.-I., Dahlin, T., Fiandaca, G., Auken, E., 2015. Measuring time-domain spectral induced polarization in the on-time: decreasing acquisition time and increasing signal-to-noise ratio. Journal of Applied Geophysics 123, 316–321. doi:10.1016/j.jappgeo.2015.08.009

Pearson, R.K., 2002. Outliers in process modeling and identification. IEEE Transactions on Control Systems Technology 10, 55–63. doi:10.1109/87.974338

Peter-Borie, M., Sirieix, C., Naudet, V., Riss, J., 2011. Electrical resistivity monitoring with buried electrodes and cables: noise estimation with repeatability tests. Near Surface Geophysics 9, 369–380. doi:10.3997/1873-0604.2011013

Revil, A., Binley, A., Mejus, L., Kessouri, P., 2015. Predicting permeability from the characteristic relaxation time and intrinsic formation factor of complex conductivity spectra. Water Resources Research 51, 6672–6700. doi:10.1002/2015WR017074

Saucier, A., Marchant, M., Chouteau, M., 2006. A fast and accurate frequency estimation method for canceling harmonic noise in geophysical records. Geophysics 71, V7–V18. doi:10.1190/1.2159063

Tables

Table 1. Duration of delay time and IP gates for the processed field data corresponding to seven gates per decade. Note that gates from 13 and higher has widths which are multiples of 20 ms.

Gate number	Delay	1	2	3	4	5	6	7	8	9	10	11	12
Width [ms]	1	0.26	0.53	0.80	1.06	1.33	2.13	2.93	4	5.33	7.46	10.4	14.4
Gate number	13	14	15	16	17	18	19	20	21	22	23	24	25
Width [ms]	20	20	40	60	60	120	120	180	300	360	540	780	1020

Table 2. Drift models included in the paper. Descriptions with sample index (n), linear coefficient (a), DC offset constant (d), sampling frequency (F_s), chargeability (m_0), relaxation time (τ), frequency exponent (*c*) and Euler's Gamma function (Γ): $\Gamma(x) = \int_0^\infty y^{x-1}e^{-u}\,dy$. Plot colors for subsequent relevant figures are also summarized.

DRIFT MODEL	DESCRIPTION	PLOT COLOR
Linear	$u_{drift}(n) = an + d$	Green
Cole-Cole	$u_{drift}(n) = m_0 \sum_{j=0}^{\infty} (-1)^j \left(\dfrac{n}{\tau F_s}\right)^{jc} \Gamma(1 + jc)^{-1} + d$	Blue or black
Instrument supplied	*Linear*	Magenta

Figures
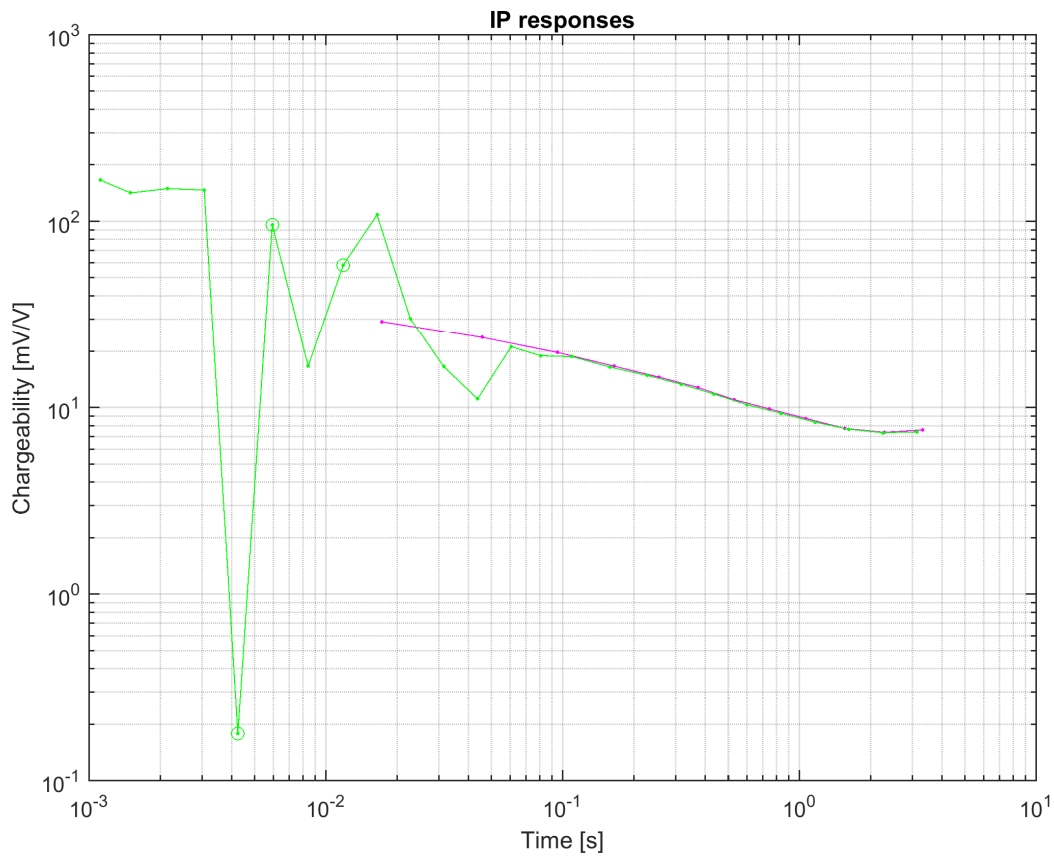
Figure 1. An IP response binned with gates that are multiples of 20 ms and delay of 10 ms (magenta, instrument output) and a re-gated IP response according to Table 1 and linear drift removal (green data points indicated by o-marker are negative). Note that the green response exhibits erratic behavior in the beginning while the gates are not multiples of the time period of the harmonic noise. Also note that the tail of both IP responses shows an increase in chargeability.
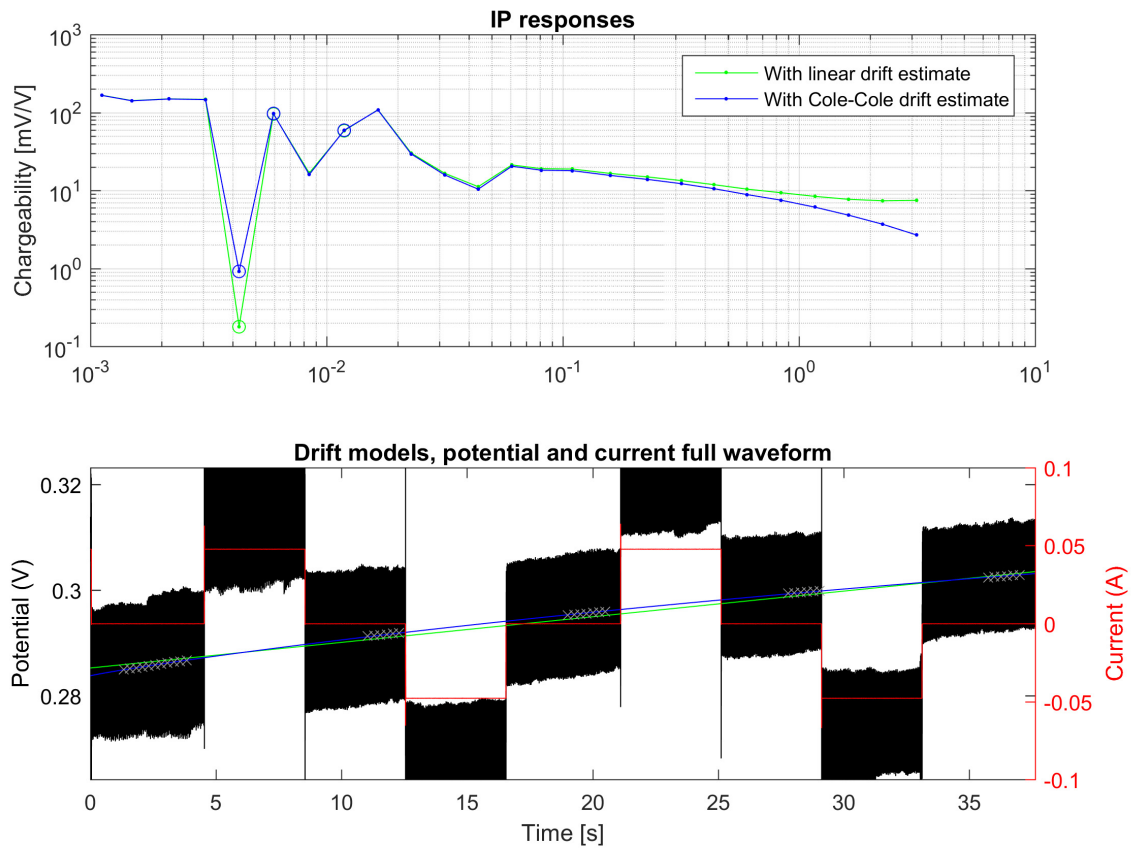
Figure 2. Bottom: 50% duty cycle raw full waveform potential (black) and current (red), subset of the signal used for finding the drift model (grey cross marker) and different types of background drift models. Top: resulting gated IP-response curves (green: linear model, blue: Cole-Cole model. Negative values are marked with circles) if no harmonic subtraction is performed. Note that the resulting shapes of the IP-responses are dependent on used drift model, especially at the end of the response.
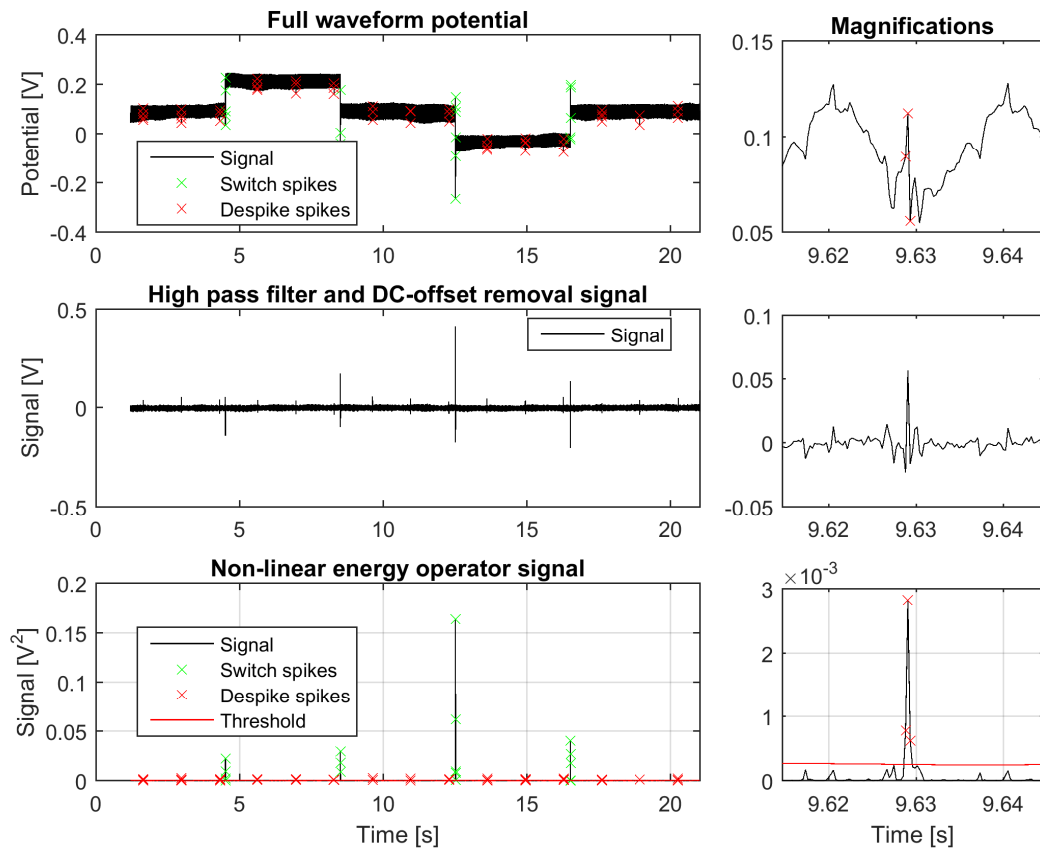
Figure 3. Identified spike samples of a full waveform potential signal (top), output from applied high pass and DC-offset removal filter (mid) and output from non-linear energy operator filter, spike samples and threshold value (bottom). Magnifications of the 7th identified spike (from 9.615 to 9.645 s) are shown on the right.
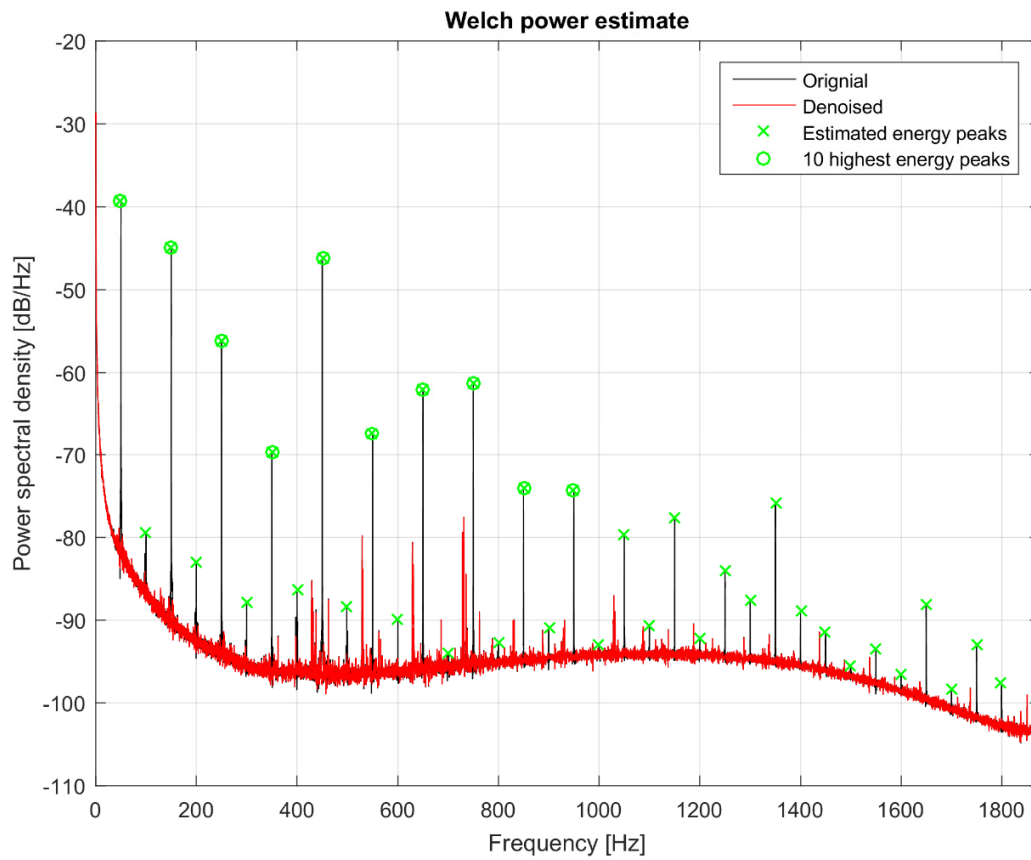
Figure 4. Welch power estimate of a full recording of potential for one quadrouple: original signal (black), residual signal after noise cancellation (red). The green markers show identified energy peaks (cross marker) and harmonics used for finding the fundamental frequency (circle marker). There is a clear reduction of the energy at 50 Hz and its harmonics after the processing and the energy level is reduced to the baseline. The remaining energy peaks are not harmonics of the 50 Hz.
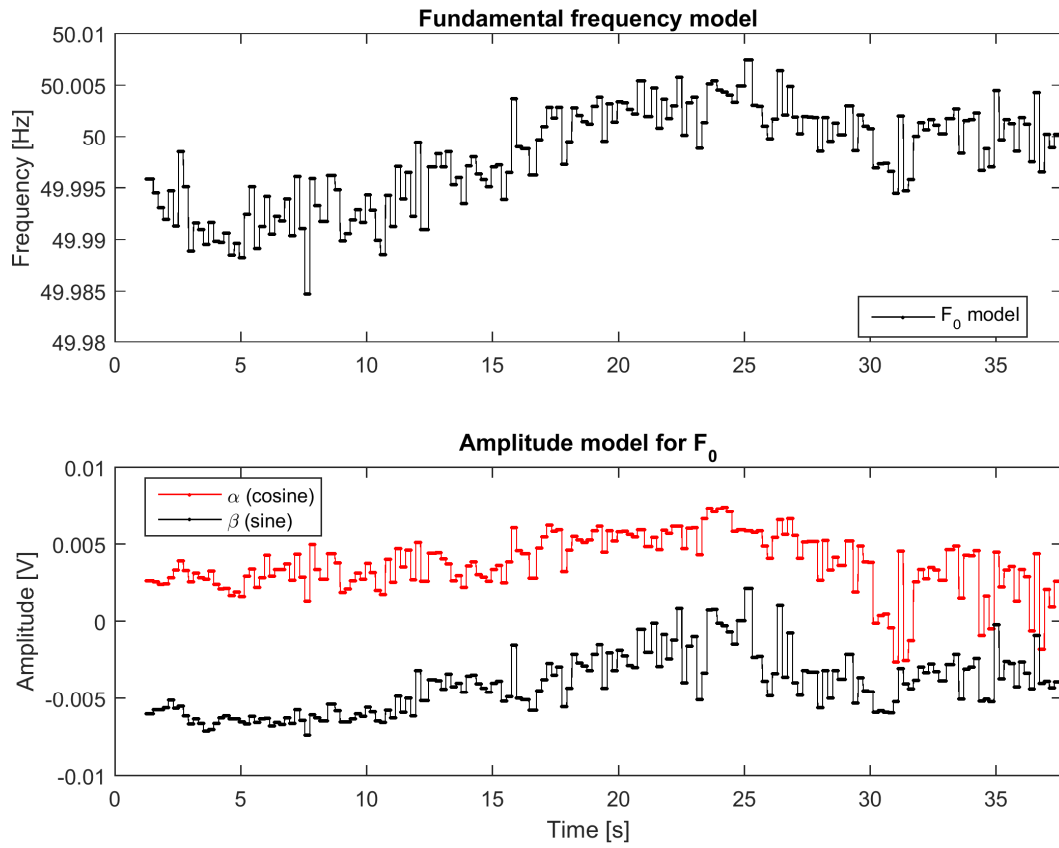
Figure 5. Example of parameters for a harmonic noise model, showing the model for the fundamental frequency (top) and amplitude models for α and β for the fundamental frequency corresponding to Eq. 5 with m=1.
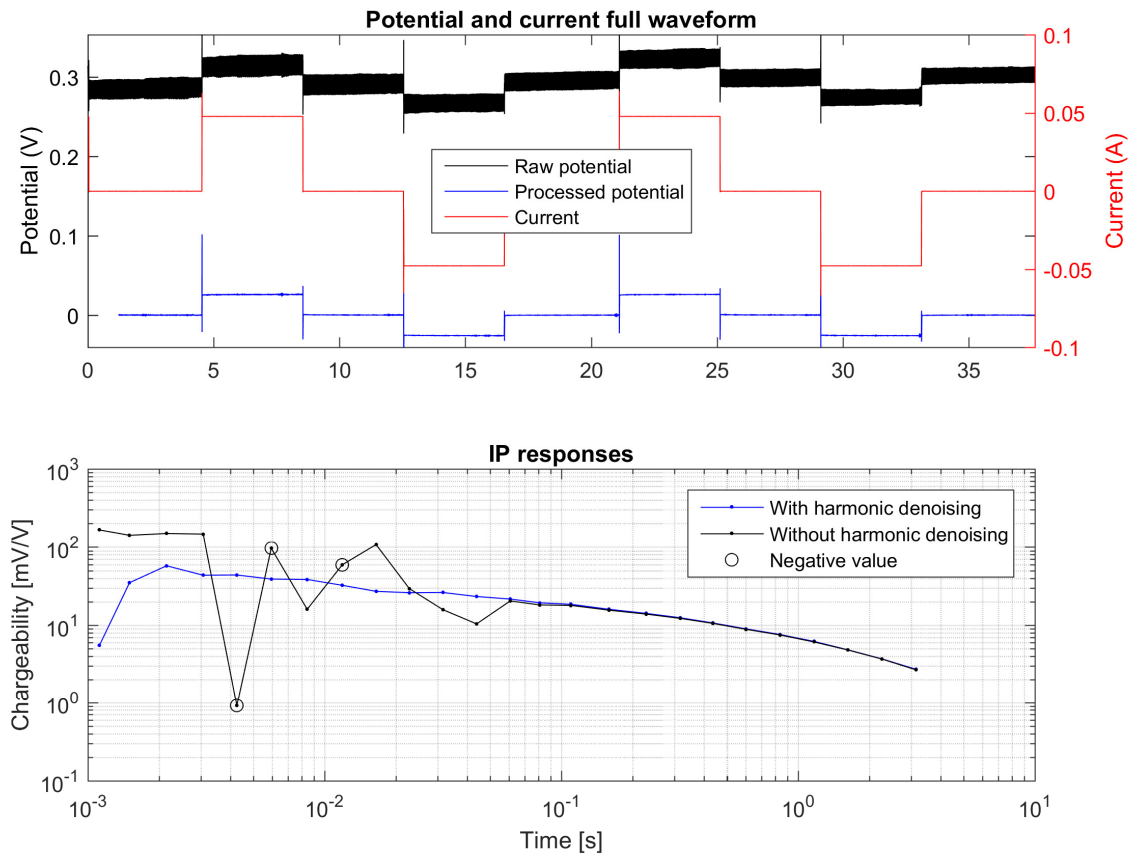
Figure 6. Full waveform current (red) and potential before (black) and after (blue) drift removal and cancelling of harmonic noise. The resulting IP responses with harmonic denoising shows clear improvement of the erratic behavior when including the harmonic denoising in the processing (bottom, blue line) compared to without (black). Model parameters examples and estimated spectral density can be seen in Figure 6 and Figure 5 respectively.
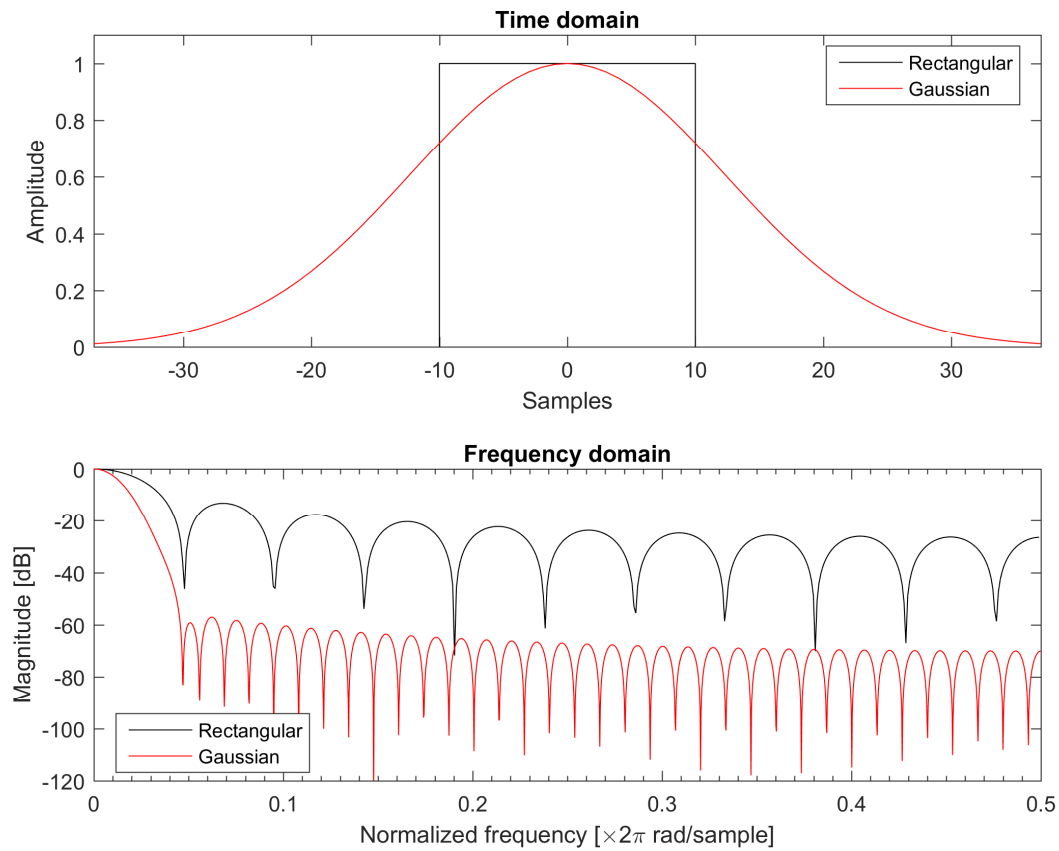
Figure 7. Time-domain and frequency-domain representation of rectangular (21 samples) and Gaussian (75 samples, σ=3) windows. Note that in frequency-domain higher frequenies is generally approximately 40 dB lower for the Gaussian window, corresponding to a factor of 100 difference compared to the rectangular window.
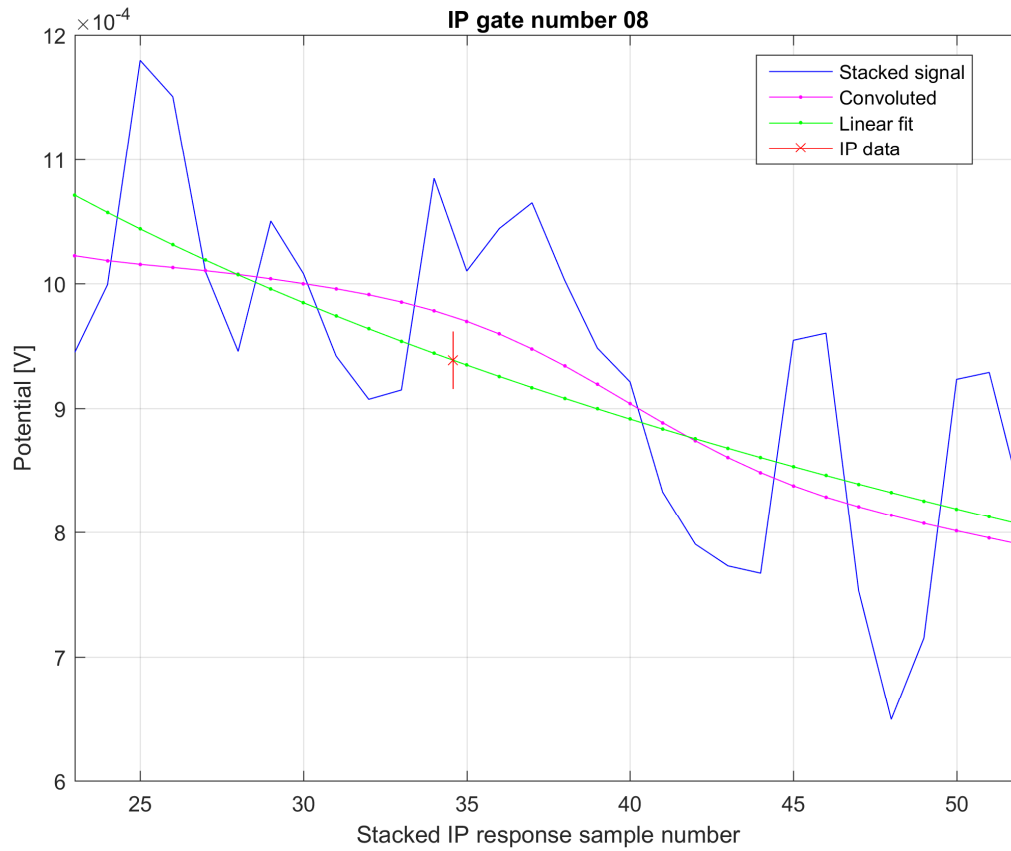
Figure 8. The different steps involved in tapered gating and error estimation for gate number 8 of the processing example. Final IP gate data with relative STD estimate of the gating corresponding to one STD are shown in red.
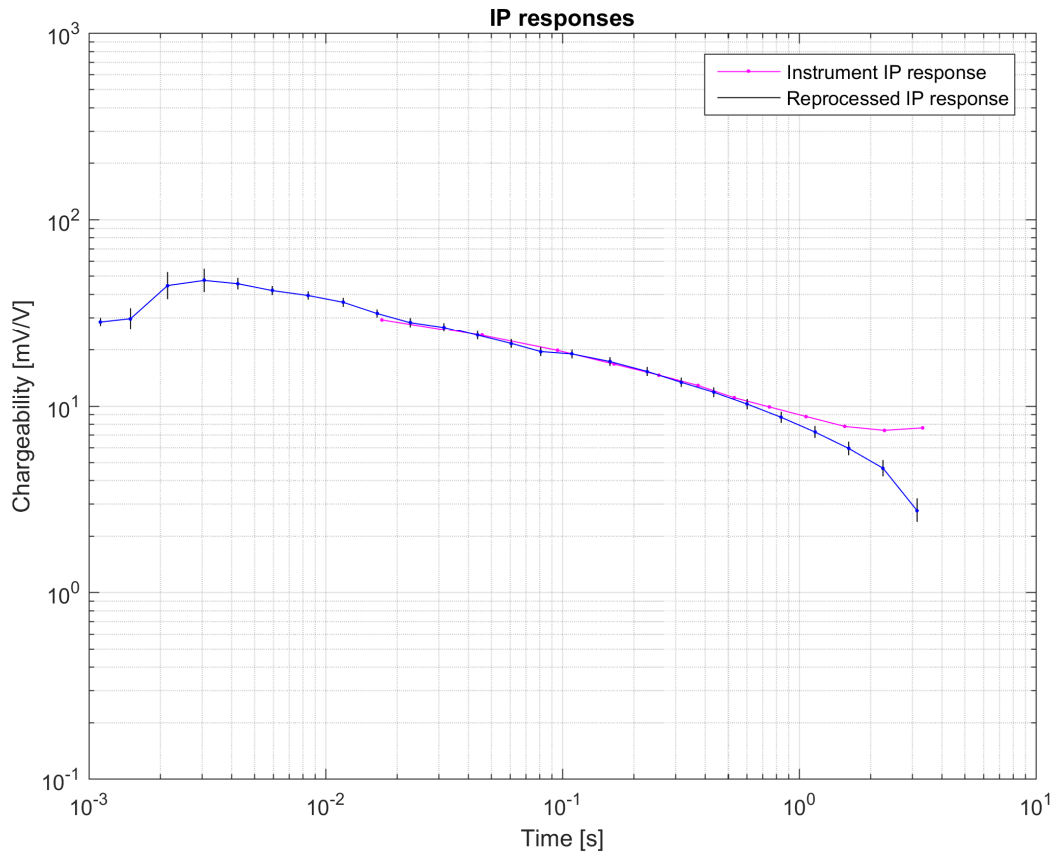
Figure 9. IP responses from instrument processing (magenta, instrument output) and the redesigned processing scheme presented by this paper (blue) with error bars corresponding to one STD (black lines). Note that the magnitude difference between the instrument and the reprocessed IP response increases at late times as a result of the poor performance of the instrument drift removal. This, together with enabling IP response information one decade closer to time zero by applying harmonic denoising and redesigned gating scheme doubles the spectra l content of the reprocessed response compared to the instrument processing.
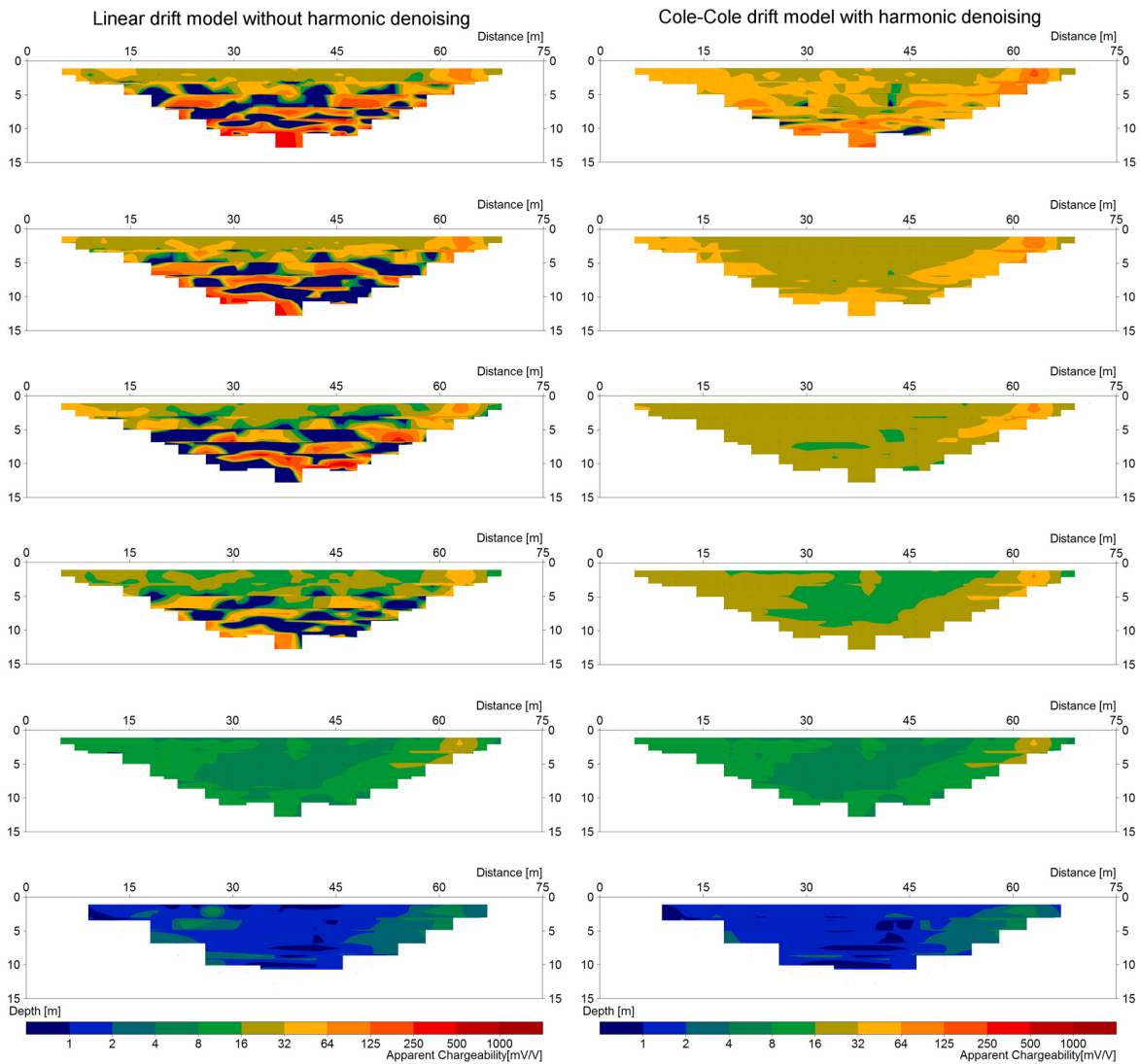
Figure 10. Pseudosections for IP gates 3, 6, 9, 12, 18 and 25 (from top-down) for processed data without harmonic denoising and linear drift removal (left) and with harmonic denoising and Cole-Cole drift removal (right) of full waveform data. The pseudosections without harmonic denoising with linear drift estimate shows an erratic behavior for all gates not multiple of the time-period of the harmonic noise as well as for the later gates due to poor performance of the linear background drift removal. Contrastingly, the processed data shows relatively smooth pseudosection already from gate 3 and an exceptional improvement for the later gates 6up to the 12th gate.